TURBULENT FLOW OVER A PIN FIN ARRAY: PARAMETRIC STUDY

By

Benjamín Cruz Pérez

A thesis submitted in partial fulfillment of the requirements for the degree of

MASTER OF SCIENCE

in

MECHANICAL ENGINEERING

UNIVERSITY OF PUERTO RICO
MAYAGÜEZ CAMPUS

May, 2010

Approved by:

Vikram Pandya, Ph.D. Member, Graduate Committee	Date
Gustavo Gutierrez, Ph.D. Member, Graduate Committee	Date
Stefano Leonardi, Ph.D. President, Graduate Committee	Date
Miguel Pando, Ph.D. Representative of Graduate Studies	Date
Gustavo Gutierrez, Ph.D. Chairperson of the Department	Date

ABSTRACT

Modern jet engines reach very high combustion temperatures to achieve higher thermal efficiencies which can damage the turbine blades. Damage can occur in the turbine blade due to the temperature difference between the interior and the exterior causing material creep and thermal fatigue. To avoid damage efficient cooling systems have been proposed such as film cooling, internal channels, and pin fins. This research focus on pin fins, which are small protruding cylinders at the trailing edge of the turbine blade, specifically the purpose of this work is to find the optimum layout of pin fins such that it enhances the heat transfer process with a minimum pressure drop. To find this optimum pin configuration experiments and numerical simulations have been performed. Experiments consisted on determine the friction factor for pin fins arrays ranging from one row to ten rows at equally spaced intervals and various Reynolds number (Re). Experiments demonstrated that for arrays with more than 6 rows of pin fins the friction factor follows a decreasing trend as the Re increases and the pressure drop due to the array to the total pressure drop ratio is about 90%. The numerical method used for the Direct Numerical Simulations (DNS) is the same presented by [1]. DNS consisted on changing the spacing between the pin fins and the Re. For a fixed spanwise distance the streamwise distance was varied and for a fixed streamwise distance the spanwise distance was varied for a constant Re. Finally, for a fixed spacing the Re was varied. The numerical results shows that the heat transfer trends to increase as the spacing between the pin fins becomes smaller, and the friction factor decreases as the spacing becomes larger. For a fixed pin configuration the heat transfer and the friction factor increases with decreasing Re.

RESUMEN

Los motores jet modernos llegan a temperaturas de combustión muy altas para alcanzar una eficiencia termal más alta que puede dañar los alabes de las turbinas. El daño en los alabes puede ocurrir debido a la diferencia en temperatura entre el interior y el exterior del alabe causando fluencia en el material y fatiga termal. Para evitar el daño se han diseñado sistemas de enfriamiento eficientes como lo son enfriamiento de película, canales internos y aletas en forma cilíndrica. Este trabajo esta enfocado en aletas con forma cilíndrica que por lo general son utilizadas en la parte tracera del alabe. El propósito específico de este trabajo es encontrar la configuración óptima que promueva la transferencia de calor a una caída de presión mínima. Para encontrar esta configuración óptima se realizaron experimentos Simulaciones Numéricas Directas. Los experimentos consistieron en determinar el factor de fricción para varios arreglos de aletas que iban desde una fila hasta diez a intervalos de espacio iguales y para un número de Reynolds (Re) variado. Los experimentos demostraron que para un arreglo de más de 6 filas de aletas con forma cilíndrica el factor de fricción decrece a medida que el Re aumenta y que la razón de caída de presión debido al arreglo en términos de la caida total es aproximadamente 90%. El método utilizado para realizar las simulaciones númericas directas es el mismo presentado en [1]. Las simulaciones consistienron en cambiar el espacion entre las aletas y variar el Re. Para una destancia a lo ancho fija se varió la distancia paralela al flujo y para una distancia paralela al flujo fija se varió el espacio a lo ancho. Finalmente para un espacio fijo se varió el Re. Los resultados numéricos muestran que la transferencia de calor tiende a aumentar a medida que el espacio entre las aletas cilíndricas se hace más pequeño y el factor de fricción disminuye a medida que el espacio incrementa para el mismo Re. Para una configuración fija la transferencia de calor y el factor de fricción aumenta cuando el Re decrece.

For the LORD gives wisdom, and from his mouth come knowledge and understanding (Proverbs 2:6, NIV)

ACKNOWLEDGMENTS

I would like to thank the National Science Foundation for providing founding for a Research Experience for Undergraduates internship at the Pennsylvania State University as part of a project led by Dr. Karen Thole. My sincere thanks to Dr. Thole for encouraging me as an undergraduate student to get into this research field. I would also like to acknoledge the funding from Pratt & Whitney which supported most of my MS graduate studies at the University of Puerto Rico Mayaguez Campus and for the internship at Infotech Aerospace Services. Teragid for computational time at Ranger supercomputer at University of Texas. Jaime Toro for been my lab partner since the begining, Josuan Hilerio, Juan Garcia, Glenn Cooper Vidal and Byron Zambrano for sharing with me their experiences. John Lucena for help in the development of some codes used during this thesis, and Amabel Reyes for giving some organization to the lab. Stefano Leonardi for advising me in the academic aspect and as a friend. Finally, but not less important, to my family for their support.

TABLE OF CONTENTS

page

LIST OF TABLES

LIST OF FIGURES

Figure page

LIST OF ABBREVIATIONS

MPI	Message Passing Interphase
DNS	Direct Numerical Simulation
CFD	Computational Fluid Dynamics
RANS	Reynolds Average Navier-Stokes
CFL	Courant, Frederich and Lewis
ExCCL	Experimental and Computational Convective Laboratory
PSU	Pennsylvania State University

LIST OF SYMBOLS

α	Thermal diffusivity
A_{ht}	Area of heat transfer
A_{ref}	Reference Area
C_D	Drag coefficient
C_P	Pressure coefficient
C_f	Friction coefficient
ΔP	Pressure difference
Δt	Time step
Δx_i	Mesh width in the i^{th} direction
D	Diameter
D_h	Hydraulic diameter
ϵ	Roughness
f	Friction factor
h	Height
j	Colburn j-factor
L	Wake length
L_D	Test section length
l_e	Entrance length
μ	Dynamic viscosity
N	Number of rows
Nu	Nusselt number
∇	Gradient operator
ν	Kinematic viscosity
ω	Frequency
P	Pressure
Pr	Prandlt number
Π	Body force
q_i	Heat flux in the i^{th} direction
Re	Reynolds number
ρ	Density
s	Specific entropy
S	Entropy
S	Spanwise distance
St	Strouhal number
St_{HT}	Stanton number
T	Temperature
τ	Time constant
τ_s	Shear stress

u_i	Instantaneous velocity component in the i^{th} direction
$\bar{U}_i$	Average velocity component in the i^{th} direction
u'_i	Fluctuating velocity component in the i^{th} direction
V	Velocity
X	Streamwise distance
x_i	Dimension in the i^{th} direction
χ	Correction factor

CHAPTER 1
INTRODUCTION

Gas turbine engines are used extensively in the aerospace industry and in energy generation. Many commercial and military airplanes employ these engines for propulsion. The main components of a gas turbine engine are the diffuser, compressor, combustor (or burner), turbine, and nozzle (figure 1–1). The air enters in to the engine through the diffuser where it reduces its incoming velocity (i.e. the velocity at which the aircraft travels) and increases the pressure. If the aircraft is not moving the effect of the diffuser is null. The air then passes to the compressor which increases the air pressure by means of transforming energy from kinetic to potential (i.e. rotation to pressure). The process of transforming the kinetic energy to potential is achieved via an arrangement of stators and blades in the compressor. Blades are rotating and add kinetic energy to the fluid. Stators remain static and convert the kinetic energy to potential energy, this change is reflected in the increase of the pressure. One set of stators and blades are know as a stage. Compressors require many stages to increase the pressure significantly. There are two kinds of compressors used in today's aircraft, they are the axial flow compressor (previously described) and the centrifugal compressor. In a centrifugal compressor the fluid enters through the rotating impeller which centrifuges the fluid to the shell. This process adds energy to the air and increases the pressure. Some of the compressor air is used to drive some engine systems (cooling system) and some aircraft systems (air conditioning, maintain cabin pressure, etc.). This process of taking compressed air from the compressor is know as air bleed.

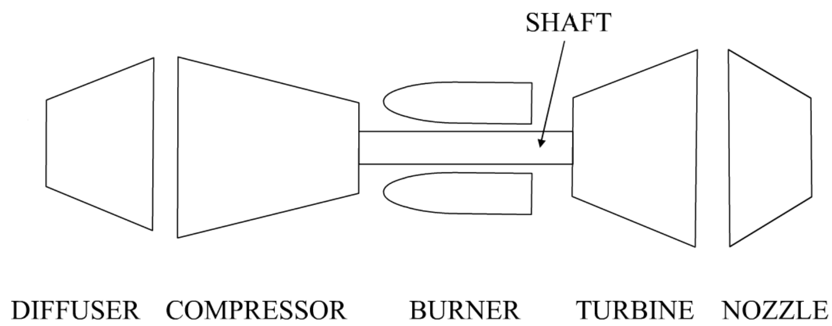

Figure 1–1: Simplified turbojet engine main parts schematic

Once the air passes through compressor, it enters in to the combustor where it is mixed with fuel and ignited. Combustion adds more energy to the air, which is accompanied by a significant increase in the temperature of the fluid. The high energy air from the combustor flows through the turbine which extracts part of the energy and transform it into shaft power. The turbine stators convert the pressure energy to kinetic energy which the blades transform into rotational shaft motion. The turbine works similar as the compressor, but with an opposite purpose. As the compressor, the turbine is composed of some stages. The shaft power obtained from the turbine is used to drive the compressor and other components of the engine such as the lubrication system. Then, the air flows through the nozzle which changes the air pressure (the remaining energy) into jet velocity. Military aircraft can change the nozzle outlet area to increase the jet velocity for higher thrust. Also, some engines had an extra part between the turbine and the nozzle know as the afterburner which take the air that exits the turbine and reheat it again by means of another combustion. Now the air contains more energy and it is used entirely for propulsion purposes.

The gas turbine engines typically run on a Brayton cycle (Fig. 1–2), and to achieve higher efficiencies the combustor exit temperature (temperature 3 in fig. 1–2) must be raised. This will increase the thermal efficiency of the cycle by making it closer to the Carnot efficiency. The increase of the combustor exit temperature

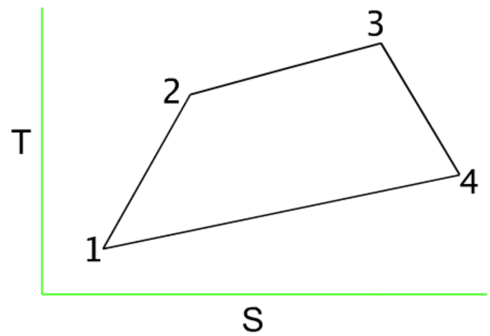

Figure 1–2: Ideal T-S Brayton Cycle showing important operating points of the jet engine (T is the absolute temperature and S is the entropy). (1) is the intake, (2) is the compression stage, (3) is the combustion stage and (4) is the exhaust stage

will increase the area inside the cycle curve and therefore more work output can be obtained from the cycle with the same energy loss.

The energy that is wasted due to inefficiencies is reflected in the temperature of the air jet that comes out from the engine. The inefficiencies are due to the components loss and thermal inefficiencies. The high temperature from the combustor can damage the downstream components of the engine (Fig. 1–3), therefore cooling systems are needed to protect the turbine stators and blades from the hot air.

Figure 1–3: Damaged turbine blade due to excessive temperature. Damage can occur when pilots do not follow manufacturer specifications.

There are two approaches mainly used in the cooling and protection of the turbine stators and blades, which are external and internal cooling. External cooling is achieved by impingement's jets in the exterior of the blade that creates a thin relative cold air film around the blade. The film prevents that the incoming hot air enters in direct contact with the turbine stators and blades. Internal cooling is obtained by the use of internal channels with turbulators and pin fins exposed to a coolant fluid flow. These channels present turbulators to improve mixing and therefore the heat transfer from the hot blade material to the coolant fluid. At the trailing edge of the stator and/or blade, cooling channels can not be accomodated therefore pin fins are placed to increase the heat transfer while providing structural support to the stator and/or blade itself [6, 7]. The typically size of a blade for aero applications is not larger than 5 cm (2 in.) by 2.5 cm (1 in.).

1.1 Justification

Modern gas turbine engines generate high temperature gases in the combustor [6] to achieve higher thermal efficiency levels and therefore more useful work output. These combustion product gases may reach temperatures hot enough to melt some engine components along their flowpath [3], especially the turbine's stators and blades, which are the first components that come directly in contact with these hot gases after the combustor. To avoid damage in the turbine blades (figure 1–3), many cooling devices have been used, such as internal passages with roughness (or turbulators), film cooling, and pin fin cooling [3, 8, 9] (fig. 1–4).

Internal cooling of the turbine stator (or blade) is achieved by increasing the turbulence levels [9, 10] in the internal passages or by increasing the wetted area (heat transfer area) inside the passages [3]. The larger these two factors the higher the heat transfer by forced convection and conduction from the hot surface to the coolant fluid, however, this also raises the pressure drop across the internal channel. A high pressure drop means that more compressor work is required to cool the stators and blades [3] by bleeding more air from the compressor, making the entire thermal

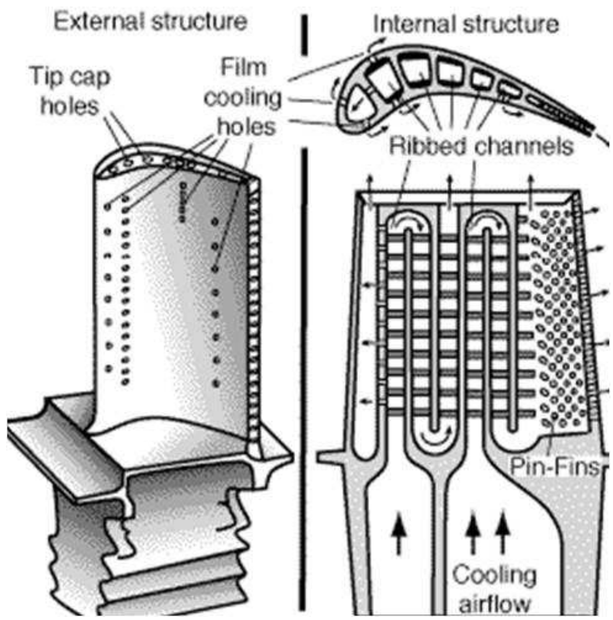

Figure 1–4: Turbine blade cooling mechanisms. Film cooling holes avoid the hot air to touch directly the blade and internal channels and pin fins provides internal heat transfer from the blade to the cooling airflow.

cycle less efficient [11]. Also, a high pressure loss is undesirable if the pressure head available in the internal channel is limited [9, 12].

Pin fins are protruding small cylinders in the interior of the turbine stator and blade trailing edge [7, 13–15]. The height of the channel (h) over the diameter (D) of the pin ranges between $0.5 < \frac{h}{D} < 4$ [14, 16]. Usually the pin $\frac{h}{D}$ is approximately 1 due to manufacturing constraints [17]. Their main purpose is to increase the heat transfer both via convection and conduction from the hot walls to the coolant fluid. The aim of the present research is to find the best layout of the pin fins array which increase the heat transfer in the pin fins without compromising the compressor efficient operation by testing different arrays and dimensions.

1.2 Objectives

The main objective of this research is to find the optimum configuration for the pin fin array which enhances the heat transfer and pursue the lowest pressure drop across the channel section. The pressure drop will be measured experimentally as well as numerically. The heat transfer will be computed numerically.

To comply with this objective several pin fin arrays will be studied and different Reynolds numbers will be also tested. In the experimental case only $\frac{S}{D} = 2.5$ and 5 will be considered, where S is the spanwise distance, with Re = 5000, 10000, 15000, 25000, and 30000, all cases with staggered configuration.

With the numerical approach different effects will be studied. To measure the effect of the Reynolds number a configuration similar to the experimental will be used ($\frac{S}{D} = 2.5$ and $\frac{X}{D} = 1.5$, X being the streamwise distance between two consecutive rows), the Reynolds number will be varied from 2000 to 6000. The effect of the streamwise spacing will be accounted by fixing the Reynolds number to 4000 and the spanwise spacing to $\frac{S}{D} = 2.5$ for $\frac{X}{D} = 1.5$, 3, 4.5, and 6. Finally, the effect of the spanwise distance will be considered by letting constant the Re to 4000 and the streamwise space to $\frac{X}{D} = 3$, the cases that will be on focus are $\frac{S}{D} = 1.5$, 2.5, 4, 6. Velocity and turbulent heat flux profiles will be presented for several cases, as well as a summary of the heat transfer capabilities of each array.

1.3 Organization of the Thesis

The thesis is organized in the following manner:

Chapter 2 - Methodology - This chapter explains how experiments were conducted and the numerical method utilized for the simulations.

Chapter 3 - Infinite Cylinder - Includes a brief study of the infinite cylinder as an understanding of the behavior of the flow and the effects of the Reynolds number on this geometry.

Chapter 4 - Flow and Heat Transfer Characteristics for Cylinder Arrays and Endwall Effects - Flow around a cylinder is affected by the upstream and downstream features, this chapter contains a literature review of the effects of having other cylinders in the flow direction and perpendicular to the flow. It also includes a brief section of channel flow.

Chapter 5 - Flow and Heat Transfer Characteristics for Pin Fins and Experimental

Studies - This chapter presents a literature review on pin fins and the experimental studies results and discussion.

Chapter 6 - Effects of the Streamwise Spacing on Pin Fins Heat Transfer and Friction Factor - Streamwise space have an effect on the behavior of the flow in an array of pin fins. Here this effects are presented and discussed.

Chapter 7 - Effects of the Spanwise Spacing and Reynolds Number on Pin Fins Heat Transfer and Friction Factor - This chapter presents the effect of the spanwise distance between the pin fins and the effects of the Reynolds number.

Chapter 8 - Conclusions and Recommendations

CHAPTER 2
METHODOLOGY

2.1 The Experimental Procedure

Experiments were conducted at Experimental and Computational Convective Laboratory (ExCCL) in the Pennsylvania State University (PSU) where I spent a summer. The test facility is the same test facility described by Lyall and Thrift [3] (figure 2–1). Leaving the blower, the air flows through 6 in. (15.24 cm) diameter piping at for a distance of 520 in. (13.208 m) before entering the plenum. In the plenum, the air flow hits a splash plate, which prevents the incoming jet from entering the test section directly. The plenum also encases a heat exchanger that provides the test section with air at a uniform constant temperature. The air enters the test section through a rounded inlet, then flows into an extension that makes the transition from duct flow to pipe flow, entering the piping again, for a distance of 21.33 pipe diameters, such that a fully developed turbulent flow enters the flow meter (orifice meter). From the flow meter, the air flows for 11.67 pipe diameters before entering the blower, and recycle again.

The test section itself (figure 2–2) was a parallel plate channel, with a width of 24 in. (609.6 mm) and a height of 0.375 in. (9.525 mm) for a height to width ratio of 64:1. The air flows for a distance of 52 pin diameters (D) before reaching the first row of pins, and then flows for another 38 pin diameters from the first row of pins to the end of the duct. Pressure taps were located 24 pin diameters upstream and 16 pin diameters downstream from the first row of pins, to ensure fully developed flow in the measuring regions. The length necessary to ensure a fully developed flow

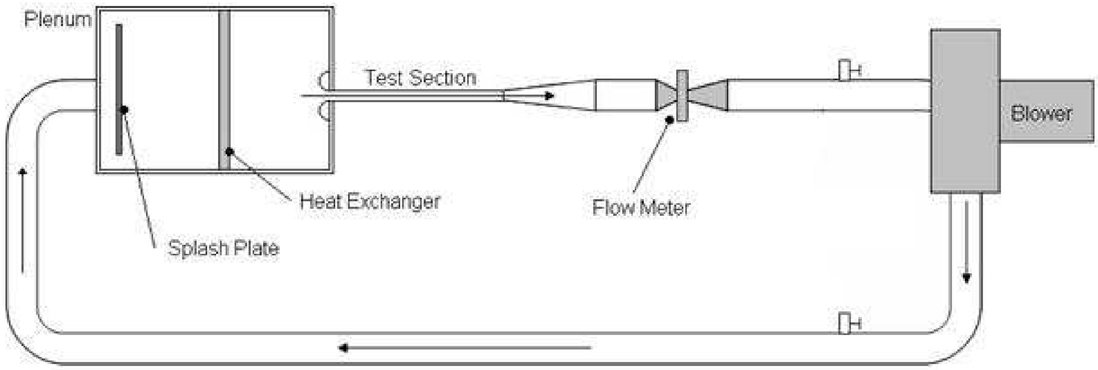

Figure 2–1: Closed loop wind tunnel used during the experiments same as [3] (arrows shows the flow direction). (Adapted from [3])

is given by:

$$\frac{l_e}{D} = 4.4Re^{\frac{1}{6}} \tag{2.1}$$

where l_e is the entrance length, D is the hydraulic diameter of the test section, and Re is the Reynolds number at the entrance [18]. This equation is valid only for turbulent flow conditions, as in the experimental cases.

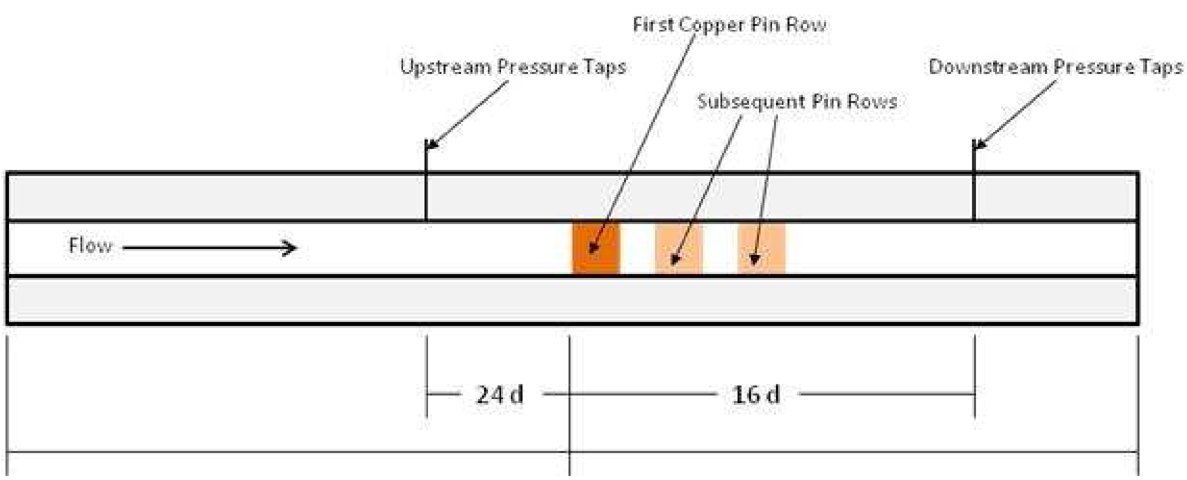

Figure 2–2: Parallel plate test section: pressure taps are located 24 pin diameters upstream and 16 pin diameters downstream to ensure fully developed flow at the measuring zones.

Figure 2–3 shows a portion of a two row, staggered pin fin array. The air flows in the x (streamwise) direction, and the rows are placed perpendicular to the flow in the z (spanwise) direction. X is the streamwise spacing between pin row centers, while S is the spanwise spacing between pin centers for pin on the same row. The staggered effect was achieved by displacing the pins in the even numbered rows by a distance of $\frac{S}{2}$ in the spanwise direction.

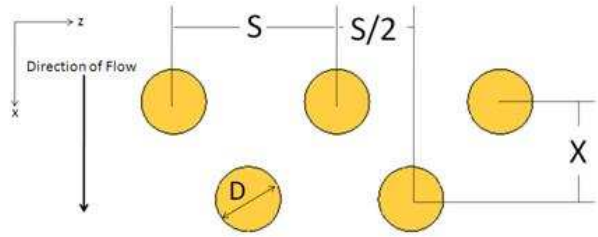

Figure 2–3: Staggered experimental pin fin configuration. S is the spanwise distance, X is the streamwise distance, and D is the diameter of the pin.

The static pressure was measured using pressure transducers connected to pressure taps at the test section. The measuring point was changed by using a scan-valve that were able to connect the tap to the pressure transducers. The signal from the pressure transducers was digitalized using a signal processor that transformed the analog signal from the pressure transducers to a digital signal. Pressure difference between a control pressure tap and the study pressure tap was monitored using LabView. The data from LabView was exported to Microsoft Excel, and the friction factor was computed for the test section.

The computation of the friction factor was made using the following equation:

$$f = \frac{2\Delta P}{\rho V^2}\frac{D_h}{NL_D} \tag{2.2}$$

where ΔP is the pressure difference between the pressure taps upstream of the pins and the taps downstream of the pins, ρ is the air density, V is the bulk flow velocity computed from the Re at the test section entrance, D_h is the test section hydraulic diameter, L is the test section length covered by the pins, and N is the current number of rows in the test section. This equation is sometimes known as Darcy friction factor [18].

2.2 The Numerical Code

Discretized Incompressible Navier-Stokes and energy equations are solved in a staggered orthogonal Cartesian coordinate system, where the typical grid (figure 2–5) is 256 x 160 x 256 in x,y,z The velocity is defined at the faces of each cell while the pressure and temperature (passive scalars) are defined at the center of each cell. The equations for the flow are:

$$\frac{\partial u_i}{\partial t} + \frac{\partial u_i u_j}{\partial x_j} = -\frac{\partial P}{\partial x_i} + \frac{1}{Re}\frac{\partial^2 u_i}{\partial x_j^2} + \Pi\delta_{1i} \tag{2.3}$$

$$\nabla \cdot u = 0 \tag{2.4}$$

where u_i is the i^{th} component of the velocity vector, t the dimensionless time given by $\frac{t{*}U_c}{h}$, x_i is the dimension vector in the i^{th} direction, P is the dimensionless pressure given by $\frac{P{*}}{\rho U_c^2}$, Re is the Reynolds number obtained from $\frac{U_c h}{\nu}$, and Π is the pressure gradient (body force) needed to maintain a constant fluid flow rate (it is only applied to the streamwise direction). The variables with * represent a dimensional unit, h is the channel half width, ν is the kinematic viscosity, and U_c is the centerline velocity. The energy equation is stated as follows:

$$\frac{\partial T}{\partial t} + \frac{\partial T u_j}{\partial x_j} = \frac{1}{RePr}\frac{\partial^2 T}{\partial x_j^2} \tag{2.5}$$

in this equation T represents the dimensionless temperature and Pr is the Prandtl number defined by $\frac{\nu}{\alpha} = 0.71$. The variable α is the thermal diffusivity of the fluid. The non-dimensional temperature is set so that the hot wall has a value of 1, the cold wall is set to -1, and the pin fins have a temperature distribution as shown in figure 2–4. The distribution resembles experimental measurements on extended surfaces [19].

The equations are discretized using central second-order finite-difference approximation in space. The scheme used to solve the equations is the fractional step method [20] and factorization method, were the viscous terms are solved implicitly

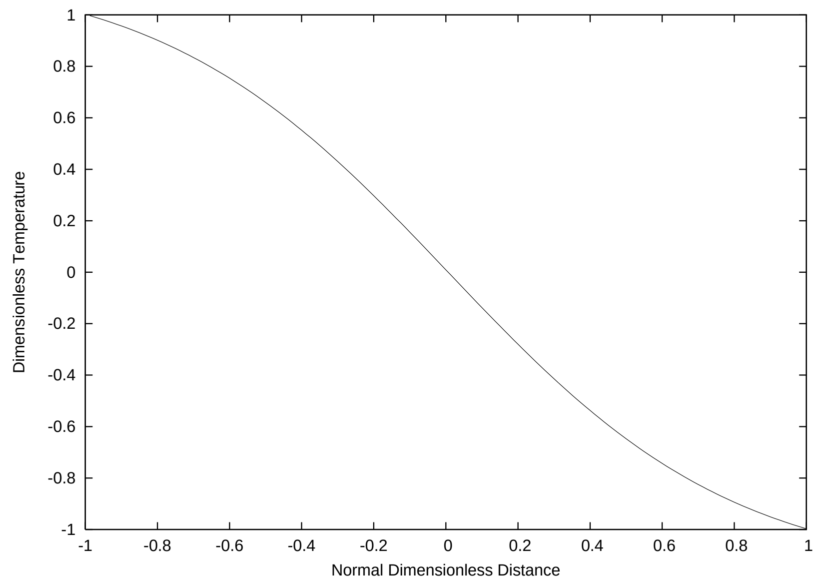

Figure 2–4: Temperature distribution for the pin fins.

and the convective terms explicitly. Stability of the numerical scheme is achieved by imposing the Courant, Friedrich and Lewis (CFL) condition given by:

$$\frac{u_i \Delta t}{\Delta x_i}|_{max} < 1 \tag{2.6}$$

where Δt is the time step and Δx_i is the mesh width in the i^{th} direction. This condition state that a particle can not move more than a grid step in the i^{th} direction in one time step. The time step is varied to provide the necessary stability to the numerical scheme and a 3^{th} order Runge-Kutta numerical integration is used to advance the solution in time.

Periodicity is applied in spanwise and streamwise directions of the computational box. To set this kind of boundary condition the values of the i_{max} are set to be equal to the $i = 1$ values. No-slip condition is set at the top and bottom walls of the channel by setting the velocity magnitude equal to zero at both walls, i.e. $u(i, 1, k) = u(i, j_{max}, k) = 0$. The immersed boundary method is applied on the body to avoid the use of body fitted grids. Body fitted grids requires a change in the coordinate system that is memory expensive and needs extra calculations to transform the data from a general curvilinear coordinate system to an orthogonal coordinate system understandable for the computer, and revert the transformation of the data to be understandable. The immersed boundary method also allows to make bodies with complicated shapes and big slope changes. It sets the magnitude of the velocity vector inside the body equal to zero by imposing a no-slip condition. To maintain the accuracy the velocity at the closest point to the body boundary are computed from a linear interpolation. Details of the numerical code are explained in detail in [1].

The code was parallelized using Message Passing Interface (MPI) routines. This allows the code to handle more data by using more fine grids than a serial code and perform computations faster by decreasing the work load to the processors. The parallelization makes the code use full advantages of clusters computers for accurate and fast processing.

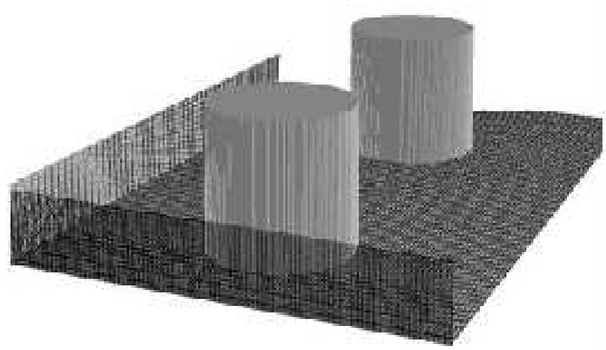

Figure 2–5: Typical grid and pin fin configuration for the numerical experiments

Post processing of the data was made using a serial code that compiles the velocity and temperature field. Since the code is parallel the data output is separated by layers. Once the field layers are put together the variables of interest are saved in memory while the next time step is read. This allows to make time averages of the fields and the variables of interest. The results of the simulations are presented in the next chapters.

CHAPTER 3
THE INFINITE CYLINDER

Flow and heat transfer of pin fins combine the characteristics of end wall and cylinder conditions [16], but the flow and the heat transfer can not be interpolated from the infinite cylinder and the plain channel flow. To have a better understanding of the flow and heat transfer characteristics of the pin fins, the cylinder effects and the endwall effects on the flow will be reviewed separately. In fact, pin fins are mainly protruding low aspect ratio cylinders from the heat transfer surface to the coolant flowpath [16]. The coolant fluid flow is perpendicular to the pin fins axis. Pin fins are mostly located at the trailing edge of the turbine blade (see figure 1–4) [13, 16]. In this region of the turbine blade, ribbed channel cannot be accomodated due to manufacturing constraints.

3.1 Literature Review

In the infinite cylinder, the flow is forced to decelerate to rest at the stagnation point at the leading edge. At this same point the pressure becomes maximum (stagnation pressure) since all the kinetic energy is converted to potential energy by the deceleration of the flow. As the flow moves around the circumference of the cylinder it is accelerated by a favorable pressure gradient increasing its velocity and decreasing the pressure. When the pressure reaches a minimum the boundary layer continues its development but against an adverse pressure gradient. Because of the adverse pressure gradient, the velocity gradient at the surface decreases and eventually becomes zero, this is know as the separation point. At the separation point of the boundary layer a wake is induced and the flow detaches from the cylinder surface. The flow in the wake is highly irregular and vortices can be observed. The point at which the boundary layer separates and the vortex formation is influenced by the Reynolds Number (Re).

The separation of the boundary layer creates vortices closer to the cylinder body. When the Reynolds number is large enough, this vortices shed from the cylinder forming a pattern of oscillating flow at a discrete frequency that is called Karman Vortex Street [18]. The frequency of the oscillation is expressed by the non-dimensional Strouhal number, which is given as:

$$St = \frac{\omega l}{V} \tag{3.1}$$

where ω is the frequency of the oscillation, l is the characteristic length and V is the flow velocity. The characteristic length for the case of the infinite cylinder will be the diameter and this will be valid for all the dimensionless numbers. In the case of a three dimensional infinite cylinder vortex stretching can occur. This phenomena decreases the moment of inertia of the fluid particles that are between vortex lines, this results in an increase in the angular velocity of the fluid elements. Vortex Stretching reflects the principle of conservation of angular momentum [21].

The heat transfer is characterized by a decrease from the stagnation point to the point of separation. When the separation point is reached, the Nusselt Number (Nu) increases as the result of the mixing in the wake region. There are several correlations where the Nu is function of Re and the Prandtl Number (Pr), several constants are adjusted depending on the Re range and the Pr, making them valid for all Re ranges [19], for example Hilpert proposed the following correlation for $Pr \geq 0.6$:

$$\overline{Nu}_D \equiv \frac{\overline{h}D}{k} = C Re_D^m Pr^{\frac{1}{3}} \tag{3.2}$$

In this case the constant C is adjusted depending on the Reynolds number range. Churchill and Bernstein proposed the following heat transfer correlation for

$Pr > 0.2$:

$$\overline{Nu}_D = 0.3 + \frac{0.62 Re_D^{\frac{1}{2}} Pr^{\frac{1}{3}}}{\left[1 + \left(\frac{0.4}{Pr}\right)^{\frac{2}{3}}\right]^{\frac{1}{4}}} \left[1 + \left(\frac{Re_D}{282,000}\right)^{\frac{5}{8}}\right]^{\frac{4}{5}} \tag{3.3}$$

These correlations are valid for a specific range of conditions and for most engineering applications are expected to have a 20% accuracy [19].

Low Reynolds Number

For low Re, vorticity is generated close to the surface of the cylinder due to the no slip condition [21]. For $Re < 2$ separation of the flow effects are negligible and conditions are dominated by friction drag [19]. As Re is increased ($Re > 4$) two small attached eddies appear behind the cylinder and they get longer as the Re increases. When $Re > 40$ the wake behind the cylinder becomes unstable and separates forming what is called a Karman Vortex Street, but for $40 < Re < 80$ the vortex street does not interact with the attached vortices. For $Re > 80$ the attached vortices start to oscillate, and finally the eddies break off alternately. Experiments shows that the Strouhal number remains close to 0.21 for all Re [21]. Tritton [2] establish the following correlation for the Strouhal number:

$$StRe = a + bRe + cRe^2 \tag{3.4}$$

The values of a, b, and c are reported for $50 < Re < 150$ in table 3–1.

Table 3–1: Values for constants a, b, and c for Tritton's correlation [2]

Reynolds Number Range	a	b	c
$50 < Re < 105$	-2.1±0.3	0.144±0.010	0.00041±0.00010
$80 < Re < 150$	-6.7±0.2	0.224±0.006	0

According to Dennis et. al. [22], the wake length is found to increase linearly with Re over the whole range from the value, just below $Re = 7$, at which first appears. They indicate an approximate linear growth with the Re of the standing vortex pair behind the cylinder in good agreement with experiments. The wake length is measured at the point where the flow velocity changes direction.

Transition

Transition of the flow occurs when the flow start to change from laminar to turbulent but it is not a fully developed turbulent flow. The transition Reynolds number in a cylinder can be lowered by introducing turbulence or perturbations to the flow or roughness on the surface of the body [23]. At the supercritical range there is evidence of a laminar separation "bubble", that is, a localized region consisting of a laminar separation, transition, reattachment and turbulent separation.

High Reynolds Number

At high *Re* the wake behind the cylinder becomes turbulent, and the pressure downstream becomes nearly constant and lower than the upstream pressure. The critical *Re* for a cylinder is about 3×10^5, were the boundary layer makes its transition from laminar to turbulent. For values lower than the critical *Re* the separation of the boundary layer occurs near 82 degrees from the stagnation point and for *Re* higher than the critical *Re* the boundary layer separates at 125 degrees and the wake becomes thinner, also when the *Re* is above the critical *Re* a sudden drag coefficient drop occurs. A decrease in the shedding frequency is generally accompanied by a decrease in drag [2]. The selected readings suggest that when *Re* goes to infinity the flow becomes close to a potential flow.

3.2 Numerical Experiments

In order to test and validate the numerical code, some literature conditions were tested to obtain the same results as a validation method. These studies were performed for a single two dimensional infinite cylinder subject to an incoming incompressible fluid flow. In all cases periodicity applies in the streamwise direction and the endwalls are sufficiently far from the body to neglect their effect.

In this two dimensional numerical study a longer streamwise distance was used for all the cases studied. The longer distance in the streamwise direction was to ensure that the downstream flow fluctuations created by the cylinder interaction dissipates. The periodicity of the channel can cause that the disturbances can enter again in the main stream affecting the results. The cases studied were a single cylinder subject to a flow Re_D of 2, 10, and 100. The results from the numerical experiment are compared to the experiments exposed in literature.

3.2.1 Reynolds Number of 2

The computational box for this case is 10D in the spanwise direction and 45D in the streamwise direction. The grid size is 220 x 600 in the spanwise and streamwise direction respectively. The grid points are uniformly distributed in the two orthogonal directions. At this Reynolds number the flow appears to be symmetrical around the cylinder which is in good agreement with literature [2, 18, 21] (fig. 3–1). The viscous effects dominates and no significant separation of the flow from the cylinder surface occurs, this allows the symmetry of the flow around the body. For this low Reynolds number the drag coefficient is approximately 6.23 using a previous result curve fit found in [24]. The curve fit for the drag coefficient is the following:

$$C_{D_{cylinder}} = 1.18 + \frac{6.8}{Re_D^{0.89}} + \frac{1.96}{\sqrt{Re_D}} - \frac{0.0004 Re_D}{1 + 3.64E - 7Re_D^2} \tag{3.5}$$

From the Direct Numerical Results (DNS) the C_D is 6.11. The drag coefficient was computed by performing a momentum balance in a control volume around the cylinder. The momentum balance is presented by [25] in a vector form as:

$$\vec{F} = \frac{\partial}{\partial t} \iiint_{vol} \rho \vec{V} d(vol) + \oiint_A \vec{V}(\rho \vec{V} \cdot \bar{n} dA) \tag{3.6}$$

where $\vec{F}$ is the force vector, $\vec{V}$ is the velocity vector, $\bar{n}$ is the unit normal vector to the control volume, vol is the volume, and A is the area of the face of the volume where $\bar{n}$ is proyected. Since a time average is used the time dependent term becomes zero and only the closed integral remains. To obtain the drag coefficient the force vector is divided by the reference area (A_{ref}) and the dynamic pressure ($\frac{1}{2}\rho V^2$).

The low difference between the experimental correlation found at [24] allow us to conclude that the numerical code efficiently matches the experiments at this low Re. The small difference is due to the fact that the code as well as the experiments require a time average of the instantaneous drag coefficient results, therefore there is a dependence on the time step to accurately obtain the same result and this could be the source of the difference. Also because of the discretization in the numerical code and the body there is a significant source of error at this low Re where the viscous drag dominates. Figure 3–1 shows a pressure color contour with over imposed velocity vectors. The velocity vectors shows the symmetry of the flow and pressure color contour shows stagnation point at the front of the body and the adverse pressure gradient at the aft of the cylinder. It also shows no separation behind the cylinder.

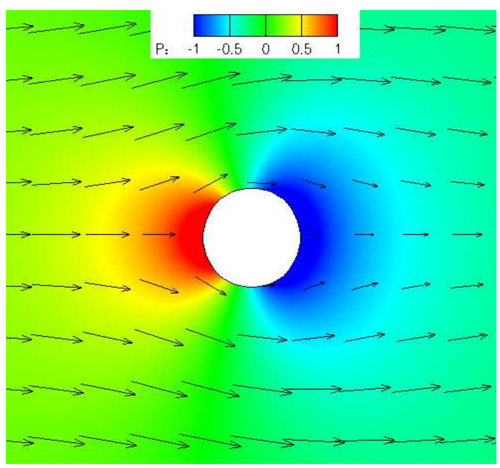

Figure 3–1: Infinite cylinder for $Re = 2$ with pressure contour and overimposed velocity vector field.

3.2.2 Reynolds Number of 10

In this case the domain is 20D and 200D in the spanwise and the streamwise directions respectively. The grid is uniformly distributed in the two directions. Figure 3–2(a) shows a pressure contour with overimposed streamlines for this case. The streamlines shows the attached vortex formation behind the cylinder as stated by [21]. The velocity vectors in figure 3–2(b) shows the decrease in the velocity in the adverse pressure gradient zone at the rear of the cylinder. The decrease of the velocity in this zone is due to the separation of the boundary layer in the cylinder surface (because of the adverse pressure gradient) and the recirculation created by the separation.

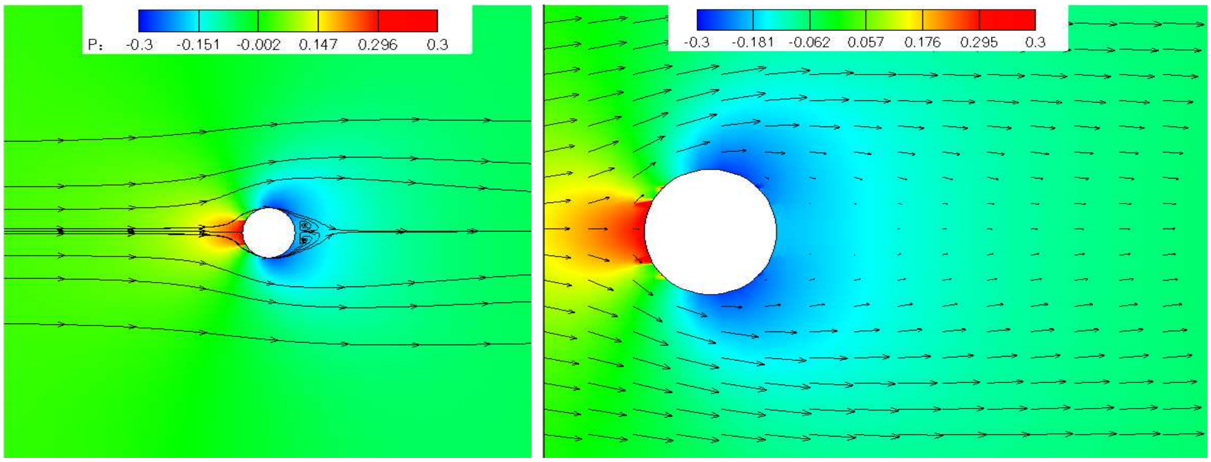

a) b)

Figure 3–2: Infinite cylinder for $Re = 10$ with pressure contour, streamlines (a) and velocity vector field (b).

Dennis et. al. [22] found that the length of the wake for a cylinder at $Re = 10$ extends for approximately 0.53D from the rear of the cylinder. The DNS experiment shows a wake length of 0.57D which is in good agreement with [22]. For this case the theoretical drag coefficient is approximately 2.67 and the computed from the DNS results is 2.71. The calculation for these coefficients was explained in the previous section. No oscillations and no eddies detachment were observed either in this case which agrees with [21].

3.2.3 Reynolds Number of 100

The domain for this case is 20D in the spanwise direction and 200D in the streamwise direction, but the grid size is larger for a more accurate calculation of the secondary flows. This distance in the streamwise direction allows the flow to develop before reaching the body again and give enough space for the secondary flows to dissipate. As established by literature the infinite cylinder at this Re produces an alternating wake (Karman Vortex Street) and detaching eddies at the trailing edge of the cylinder [2, 21]. Figure 3–3 shows the streamwise instantaneous velocity streamlines. The streamlines shows the oscillations of the flow downstream the cylinder. The pressure color contour shows how the pressure field is affected around the cylinder by the flow oscillations in contrast with lower Reynolds numbers. The low pressure spots downstream the cylinder shows the detached eddies and the Karman vortex street formed by the oscillations.

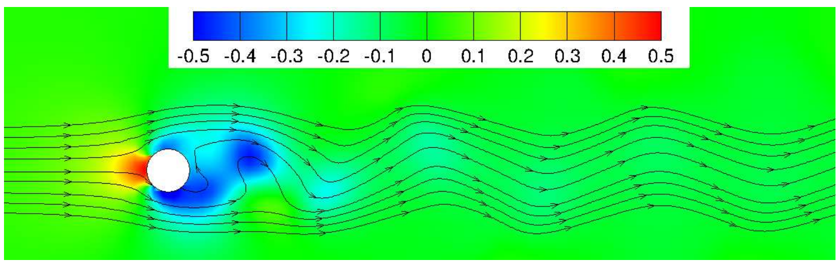

Figure 3–3: Infinite cylinder in an instantaneous pressure color contour with over-imposed velocity streamlines. Streamlines shows the oscillation of the flow past the cylinder.

The method employed to measure the fluctuation of the velocity was by setting a probe (which numerically means to save the velocity at each time step) at 11D downstream from the center of the cylinder. The probe data is plotted and the peaks are counted to obtain the frequency of the fluctuations for an arbitrary range were the flow is steady. When the flow is steady the frequency of the oscillations will be the same no matter the range taken. Finally the St is computed using as a characteristic lentgh the diameter of the cylinder and the average velocity of the fluctuations. From the data plotted in figure 3–4 the frequency of the flow fluctuations can be computed. To obtain the frequency of the fluctuations the peaks at the plot are counted and the divided by the time. The frequency (ω) for this case is 0.86 $\frac{1}{\tau}$, for a Strouhal number (St) of 0.162. The value given by literature [2] gives a St of 0.164 which is certainly close to the present simulation. The drag coefficient obtained from the DNS for this case is 1.426 while the theoretical drag coefficient is 1.449 obtained from [24]. The wake lentgh in this case could not me measured since the vortex dettachment causes that the wake become smaller in the time average. Also some of the authors [22, 23] used a splitter plate to avoid the oscillations when measuring the wake length and this obviously will affect the wake length during the experiments.

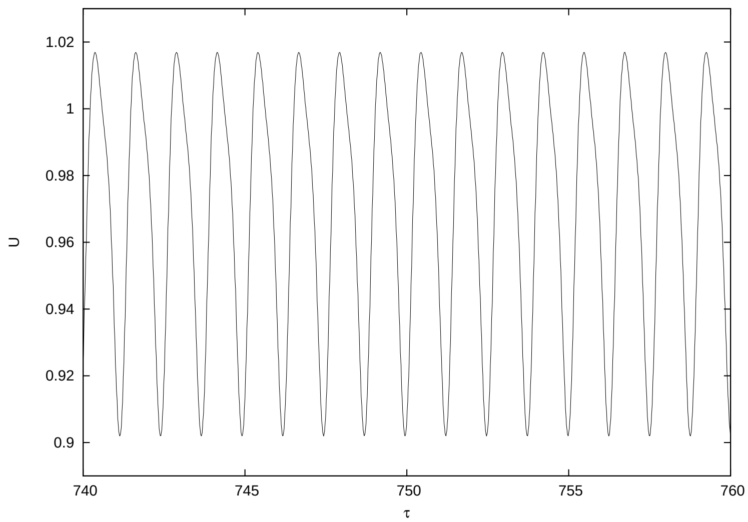

Figure 3–4: Infinite cylinder downstream streamwise velocity fluctuation with respect to time at 11D from the center of the cylinder. U represents the streamwise velocity and τ represents the dimensionless time. The frequency (ω) is 0.86 $\frac{1}{\tau}$

3.3 Concluding Remarks

This chapter focused on the infinite cylinder and its effects on a free flow. It was shown that for very low Re separation from the cylinder surface did not occurred and as the Re was increased two attached vortex appeared behind the cylinder. For higher Re the vortex start to oscillate and separates forming what is called a Karman Vortex Street. These numerical experiments have proven that the numerical code certainly produces the same results as those in literature. This is one of the standing points to prove the validity of the code.

CHAPTER 4
FLOW AND HEAT TRANSFER CHARACTERISTICS FOR CYLINDER ARRAYS AND ENDWALLS EFFECTS

It is important to understand the flow behavior and heat transfer in a cylinder array and the endwalls features before studding the pin fin arrays. At some point the pin fins behave like cylinder arrays but with the added effect of the endwall. In cylinder arrays flow conditions are affected by the upstream rows interactions and therefore the heat transfer is also affected by the same phenomena. Long cylinder arrays are mainly used in crossflow heat exchangers [6, 13].

4.1 Literature Review of Cylinder Arrays

In the case of cylinder arrays the flow conditions are dominated by boundary layer separation and wake interaction between the downstream cylinders [19]. Their length to diameter ratio is large enough so that the flow around the array can be considered external [4, 16]. Gunter and Shaw [26] proposed a friction factor correlation for an array of bare tubes with different configurations. They also concluded that their correlation can be extended to heat transfer. The pressure drop is also correlated with the friction factor and a correction constant [19] as follows:

$$\Delta P = N_L \chi \left(\frac{\rho V_{max}^2}{2} \right) f \tag{4.1}$$

where ΔP is the pressure drop in the section, N_L is the number of tubes in the bank, χ is a correction factor based on experimental data, V_{max} is the maximum fluid velocity and f is the friction factor. At low Re the friction factor is dominated by the friction drag and for higher Re the friction factor is due to the form drag [8] as for the infinite cylinder. The friction factor tends to decrease as the Re increases [26] and it resembles the drag coefficient of an infinite cylinder.

Long cylinder arrays are used when the heat transfer is the major concern [14]. The heat transfer for the first tube is almost equal to that of the infinite cylinder, but the heat transfer at the downstream rows is increased until the 4th or 5th row where the convection is stabilized [19]. The heat transfer is more significant in the cylinder surface than in the endwalls [16, 17]. In this case the effects of the endwalls are unimportant [6, 27, 28], since the cylinders provide most of the heat transfer area [4, 6]. There are, as for the infinite cylinder, several correlations for the heat transfer for both, inline configurations and staggered arrays [19].

4.2 Literature Review of Endwall Effects

The flat wall flow is well correlated in literature. For laminar flow Blasius used a similarity method to find the analytical velocity profile at various downstream positions [21]. With this solution the friction coefficient for the flat plate can be approximated by:

$$C_f = \frac{0.664}{Re_x} \tag{4.2}$$

where C_f is the friction coefficient and Re_x is the local Reynolds number [18, 21]. As the Re becomes higher the flow shows a transition to turbulent flow.

For duct flow, the laminar analytical solution is known as Poiseuville flow. The transition Re in duct flow is approximately 4000 and it is characterized by fluctuations in the parameters and randomness. Mixing is promoted by turbulence, this enhances the heat and mass transfer [18]. The Colebrook equation is used to obtain the friction factor in pipes, also the Moody chart is graphical representation of this equation which is:

$$\frac{1}{\sqrt{f}} = -2.0log\left(\frac{\frac{\epsilon}{D}}{3.7} + \frac{2.51}{Re\sqrt{f}}\right) \tag{4.3}$$

here f represent the friction factor, Re is the Reynolds number in the pipe, D is the diameter of the pipe, and ϵ is the roughness [18].

Endwalls have an important effect on the flow and heat transfer of cylinders. The endwalls are present in almost all applications of the cylinder array heat exchanger, from shell and tube and compact heat exchangers to air conditioners and refrigerators. Cylinders in heat exchangers are placed and hold by the endwalls see figure 4–1. The cylinders provides an extended surfaces for the endwall, which increases the heat transfer area of the endwall [19]. They provide more heat transfer from the solid to the fluid, first by conducting the heat through the solid extended solid (cylinders) and by convection from the surfaces of the solid [19].

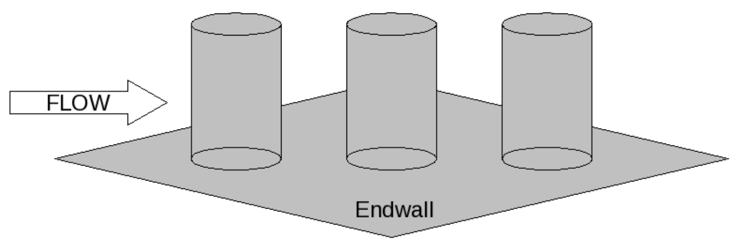

Figure 4–1: Schematic of a cylinder array with the endwall.

There is an interaction between the boundary layer of the cylinder and the endwall that causes a three dimensional secondary flow. A horseshoe vortex is the main secondary flow in this interactions [29, 30]. This feature adds another problem to the study which is the wall boundary layer behavior [29]. The flow is forced to reattach to the wall due to the strong downwash effect of the horseshoe vortex, this forms a recirculation region in the rear of the cylinder [30]. The heat transfer varies as the distance between the walls becomes closer, i. e. by making the aspect ratio $(\frac{L}{D})$ of the channel smaller. The main effect of the aspect ratio is the change in heat transfer at the aft of the cylinder [29].

4.3 Numerical Experiments on Plain Channel Flow with $Re = 4000$

The channel flow and heat transfer was simulated for $Re = 4000$. This Re is in the turbulent region for a channel flow. A turbulent flow is characterized by velocity fluctuations from the mean flow and eddying motions [25]. The results will be used as a base for understand how much the friction factor and heat transfer augments with the addition of pin fins to the channel. Channel friction factor and heat transfer are well correlated in literature [18, 19] and are very used in engineering design of pipe systems and heat exchangers. The channel is periodic in the spanwise and streamwise directions and at the upper and lower walls no slip condition is applied.

4.3.1 Mean Flow

The mean flow is characterized by high velocity at the center of the channel and boundary layer development in the near wall region. The boundary layer development is mainly due to the viscous effects of the fluid on the body surface [25]. Due to the velocity gradients in the boundary layer the shear forces are large in this region, and they are augmented in a turbulent flow [25]. Figure 4–2 shows the time averaged streamwise velocity profile for a duct flow.

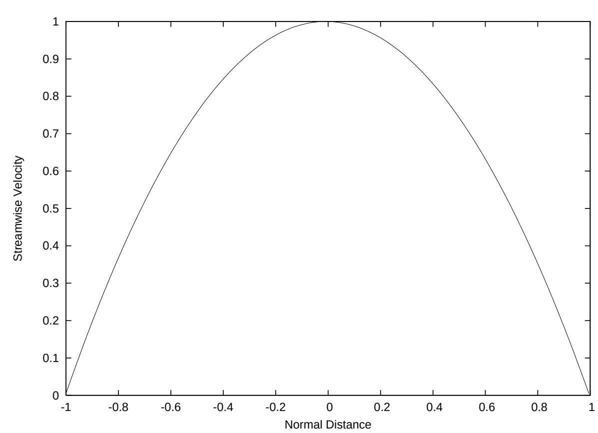

Figure 4–2: Average streamwise velocity profile for $Re = 4000$.

4.3.2 Time Dependent Terms

The instantaneous flow show velocity fluctuations at various regions of the domain and it can be described as follows:

$$u_i = \bar{U}_i + u'_i \tag{4.4}$$

where u_i is the instantaneous i^{th} velocity component, $\bar{U}_i$ is the mean i^{th} velocity component and u'_i is the i^{th} velocity fluctuation [25]. If the mean flow is subtracted from the instantaneous flow then the velocity fluctuations can be captured. Turbulent flows are characterized by random velocity fluctuations. Figure 4–3 shows the instantaneous velocity in the three orthogonal directions with its respective mean velocity.

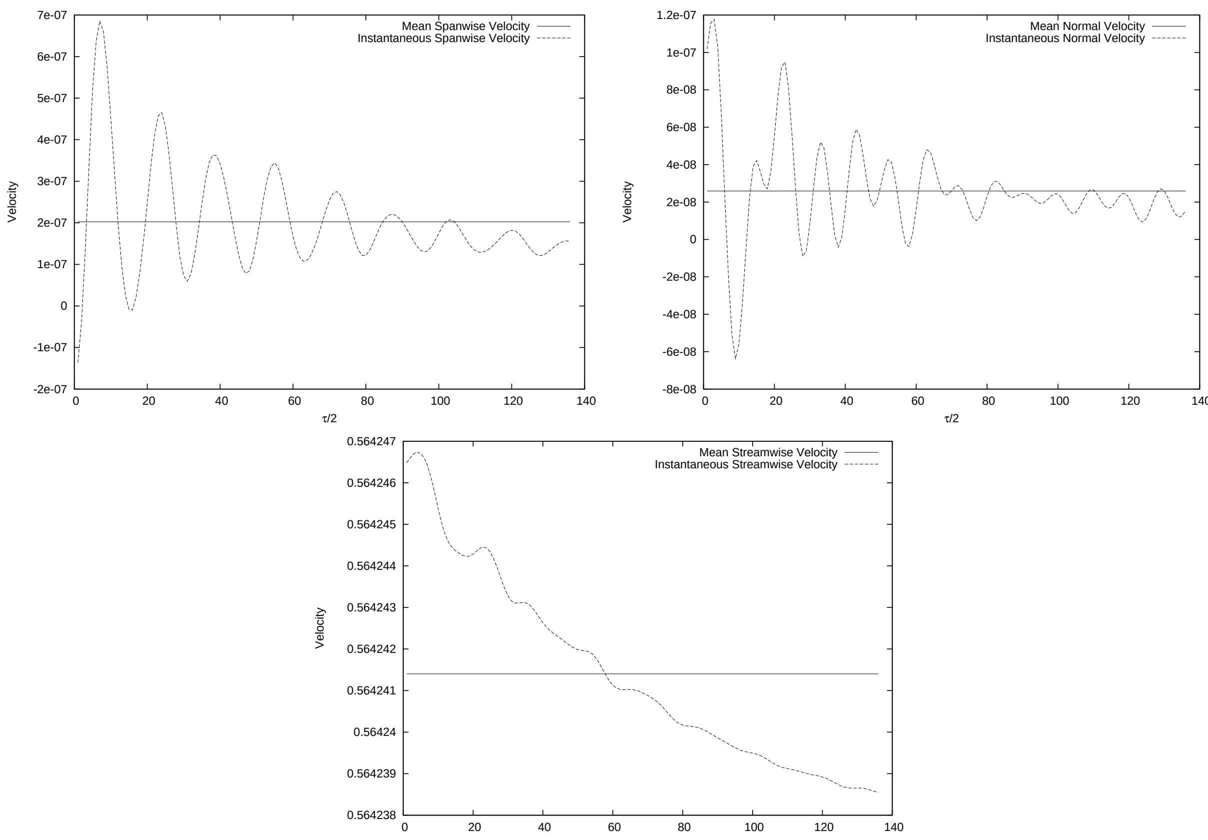

Figure 4–3: Instantaneous velocity in the orthogonal directions for a duct flow in a point at 0.25 from the main dimensions and $Re = 4000$

4.3.3 Heat Transfer and Friction Factor

The heat transfer in the case of the plain duct flow occurs from the hot wall ($T = 1$) to the cold wall ($T = -1$). This occurs via molecular conduction and convection (radiation heat transfer is neglected). Molecular conduction is given by the dimensionless Fourier's Law as:

$$q_i = \frac{\partial T}{\partial x_i} \tag{4.5}$$

where q_i is the heat flux in the i^{th} direction and T is the dimensionless temperature [19]. The molecular condition occurs mainly at low velocity zones where convection heat transfer is negligible and the only remaining mean of heat transfer is conduction since the heat flux is constant into the section. The convection is denoted by the turbulent heat flux which is a dimensionless quantity that accounts for the temperature passive scalar transport in the convective terms of the temperature transport equation. The turbulent heat flux is lower at the nearwall regions where the velocity is low and conduction dominates (fig. 4–3). It increases gradually as the center of the channel is reached, at the center of the channel it reaches a maximum and finally decrease again.

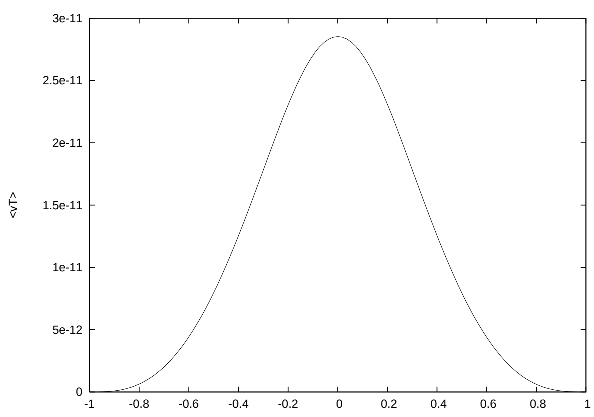

Figure 4–4: Average turbulent heat flux ($< vT >$) for $Re = 4000$.

The friction factor represents the energy loss due to the viscous effects produced in the no-slip walls. The friction is function of the shear stress and is given by:

$$C_f = \frac{2\tau_s}{\rho U_\infty^2} \tag{4.6}$$

where C_f is the friction coefficient, τ_s is the shear stress at the surface, ρ is the density of the fluid, and U_∞^2 is the bulk velocity [19]. The shear stress at the surface is computed as:

$$\tau_s = \mu \frac{\partial u_i}{\partial x_i}|_{x_i=0} \tag{4.7}$$

Here μ is the dynamic viscosity and u_i is the velocity component in the i^{th} direction that is parallel to the surface of the body [19]. Shear stresses are produced by the velocity gradient generated at the near wall region. By computing the shear stress along the channel for one wall it was found to be 0.00999835. The friction coefficient for the same duct flow is 0.03999983, this value is very close to the Colebrook equation solution which is 0.039907. The similitude between the values of the friction coefficient validates once more the numerical method due to its resemblance to experiments.

4.4 Concluding Remarks

Upstream cylinders affect the flow on downstream cylinders by affecting the wake separation and interaction between them. Flow through infinite cylinders is well correlated in literature [19]. In case of long tube banks, common in heat exchangers, the endwalls effects are unimportant because the contribution to the pressure drop and heat transfer is negligible since the cylinders contribute most of the two factors mentioned.

Duct flow was tested to prove once again the validity of the code and it will be used as a baseline for the friction factor and the heat transfer when reporting results from the pin fins. It was found a good correlation between literature friction factor and present results.

CHAPTER 5
FLOW AND HEAT TRANSFER CHARACTERISTICS FOR PIN FINS AND EXPERIMENTAL STUDIES

Many researchers and engineers have focused their efforts in measuring experimentally the heat transfer and the pressure drop for a pin fin array because the pin configuration provides a means to reduce the flow friction loss and maintain a reasonable high heat transfer. Modest work has been done trying to study the flow, the pressure drop, and the heat transfer characteristics for different pin fin arrays and shapes numerically. This is because the relative pressure drop across the pin fin bank is often small compared with other flow restrictions such as impingement slots [5].

5.1 Literature Review

The pressure drop in a pin fin array is in many cases represented by a dimensionless friction factor [10], as well as the heat transfer is presented as the Nu. The average heat transfer is usually lower than the long cylinder [3, 13, 17] but it is higher than a plain channel [11]. To have a better understanding about how the flow behaves in a pin fin array, first a single circular pin fin and then one row of pin fins will be reviewed before entering in full detail of pin fins arrays with more than one row.

5.1.1 Single Circular Pin Fin

Goldstein et al. [31] states that for a single protruding small cylinder when the fluid reaches the stagnation point, the velocity decreases and the pressure increases.

This lower velocity inside the boundary layer around this cylinder produces a small increase in pressure, resulting in a favorable pressure gradient. The pressure field causes the fluid to skew around the pin in a helical fashion [31], forming a horseshoe vortex. Han [16] claimed that significant boundary layer disturbance is generated by this wall protrusion and therefore the heat transfer is enhanced by the turbulence generated. Experimental visualization techniques has shown a horseshoe vortex formation around the pin fin [31].

5.1.2 One Row of Circular Pin Fins

Lyall and Thrift [3] concluded that the pressure drop measurements indicate that a larger friction coefficient occurred at the smaller spanwise pin spacing. They reported that the friction coefficient augmented with an increase in the Reynolds number. The heat transfer showed higher augmentations at lower Reynolds numbers, and closer pin spacing. They found that the maximum heat transfer occurred downstream of the row for lower Re and moves closer to the row as the Re was increased.

5.1.3 Circular Pin Fin Arrays

Pin fin arrays have two common array structures: inline and staggered [14]. In the inline array all pins are aligned in the streamwise direction and the spanwise direction, i.e. the distance between the pin fins center and rows is the same. For the staggered array the even rows are displaced by a certain distance (usually half wavelength) in the spanwise direction. In an empty tunnel the Nusselt (Nu) number is higher at the beginning of the thermal boundary layer and it decays to its fully developed value, in the case of pin fins arrays the Nu gradually increases to its fully developed value [16]. Heat transfer is also affected by the pin spacing in the array [16, 17]. Sparrow and Ramsey [32], Metzger and Haley [17], and Metzger et. al. [27] agreed that the transfer coefficients (mass and heat) vary at the initial rows and then reaches a fully developed value downstream.

Metzger et. al. [6] estimates that the pin heat transfer surface coefficients doubles the endwall coefficients, on the other hand Chyu et. al. [7] concludes that the heat transfer in the pin fins is 10 to 20 percent higher than the endwall. The orientation with respect to the mean flow affects the heat transfer and the pressure drop for pin fin arrays [6]. According to [5], in their review of pin fins, several researchers has developed correlations on heat transfer for staggered pin fin banks, they show dependence on Re and later correlations on the streamwise pin spacing. They [5] also evaluated the correlations with published data to prove their accuracy to at least 20%. Ames et. al. [10] studied the turbulence levels on pin fins arrays and its effect on the heat transfer, they also made a correlation that relates the turbulence levels, the heat transfer, and the Re.

Uzol and Camci [9] concluded that the wakes from the first pin fin row affect the flow at the second row resulting in an earlier separation and creating large wake zones behind the second row. These large wakes result in larger pressure drop in the array. They also report that circular pin fins have smaller pressure drops than any other shape. Han [16] states that for circular staggered fin arrays the friction factor decreases as the Reynolds number increases. Furuya et. al. [33] found that the flow for staggered short wires exhibit a three dimensional nature due to the secondary flows. Metzger and Haley [17] also corroborates the three dimensionality of the flow for low aspect ratio pin fins due to the endwall effects.

Sparrow and Ramsey [32] calculated a pressure coefficient, K_P, for an array of pin fins with a gap on the top wall, defined as:

$$K_P = \frac{\Delta P}{\frac{1}{2}\rho V_{max}^2 N} \tag{5.1}$$

where ΔP is the pressure drop across the pins, $\frac{1}{2}\rho V_{max}^2$ is the dynamic pressure and N is the number of rows. They found that K_P is strongly affected by $\frac{H}{D}$, and concluded that the pressure drop increases by a large multiple with an increase in the cylinder height. Peng [12] also agrees that the friction coefficient varies with the pin height. Arora and Abdel-Messeh [34] worked with partial length pin fins and their conclusions shows that the heat transfer can be interpolated from the smooth channel and the full length pin fins. Also the friction factor is smaller than for the full pins.

Damerow et al. [35] observed that $\frac{h}{D}$ on staggered pin fin arrays has no effect on the friction factor, which contrasts with the data presented by Sparrow and Ramsey [32]. Also they found a friction factor correlation made by Metzger et. al. [4] with a fit of ± 15 percent. Finally, they conclude, that Metzger et. al. [4] correlation is an acceptable approach for the staggered array flow friction. Peng [12] concludes that cross flow pins produce more heat transfer but also more friction loss. Ames and Dvorak [15] investigated the flow physics of pin fin array, they also used Computational Fluid Dynamics (CFD) to predict the heat transfer and the pressure drop, they found that the CFD predictions underestimated the measured values. Cruz-Perez et. al. [36] studied the flow for various rows of pin fins arrays and compared the pressure drop from experiments with Direct Numerical Simulations (DNS), obtaining a trend for 5 or more rows of pin fins. They found that for more than five rows the friction factor only depends on the Re and not in the number of rows.

5.1.4 Other Shapes Pin Fin Arrays

Other researchers have worked with non-circular and/or non-uniform pin fin shapes. Oblong pin fins where studied by Metzger et. al. [6], they conclude that heat transfer is augmented by 20% over the circular pin fins. Chyu [28] worked with pins with endwall fillets finding that the array average heat transfer is decreased and the friction factor is greater than the straight pin array. He also computed a performance index concluding that the straight in-line array performs better than the other cases studied. Goldstein et. al. [11] worked with stepped diameter pin fins concluding that this kind of pins offers more mass transfer and less resistance to the flow. Chen et. al. [13] made experiments with drop shaped pins finding that the heat transfer is lightly higher than the circular pin fins and the pressure drop is less when compared to the circular pins.

Şara [14] investigated the use of square cross-section pin fins in an staggered array, the results from this research shows that the heat transfer is improved and the friction factor is increased when compared to the smooth channel. Koşar et. al. [8] experimented with micro pin fins and low Re concluding that the conventional correlations for friction factor are inaccurate. Uzol and Camci [9] worked with elliptical pins, they concluded that the average heat transfer is 27% lower than that relative to circular pins, the elliptical pins shows less pressure drop than the circular pins (46.5% and 59.2% less for the cases studied). [9] calculated a performance coefficient that are 1.49 and 2.0 higher than the circular fins for the cases studied, turbulence levels was also studied. The performance index is the relation between the heat transfer and the friction factor and is given as:

$$\frac{N\bar{u}_D/N\bar{u}_0}{(\bar{f}/\bar{f}_0)} \tag{5.2}$$

where the $N\bar{u}_0$ is determined from the plain channel flow and $\bar{f}_0$ is computes from the Blasius power-law correlation for turbulent duct flow [9].

5.2 Experimental Results and Discussion

The present experimental results show very good agreement with literature. Figure 7–12 shows the experimental results for the friction factor for 10 rows compared with Metzger et. al. [4] correlations. This was used as a validation method for the measuring instruments and the set up used during the experiments. The correlations stated at [4] are:

$$f = 0.317Re^{-0.132} \tag{5.3}$$

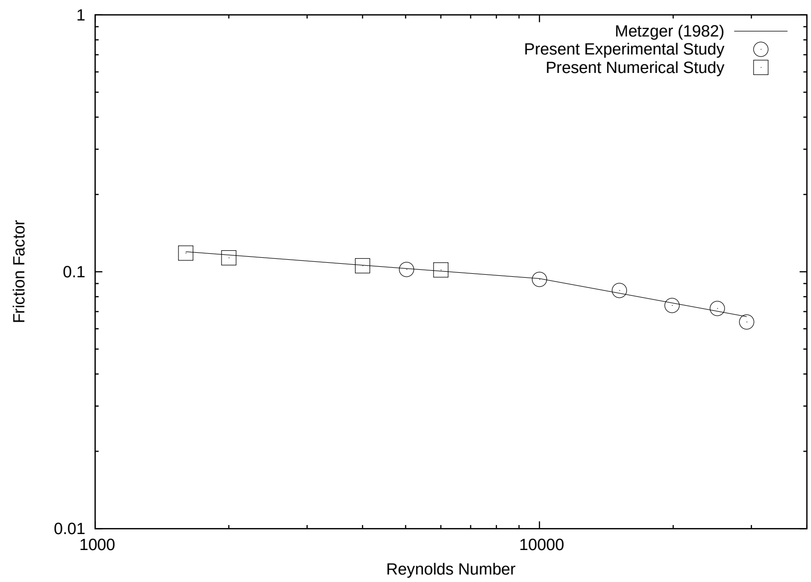

Figure 5–1: Present study experimental and numerical friction factor results plotted along with Metzger et. al. [4] correlations.

where f is the friction factor and this correlation is valid for Re from 10^3 to 10^4 and

$$f = 1.76Re^{-0.318} \tag{5.4}$$

that is valid for Re from 10^4 to 10^5.

From figure 7–12 it can be concluded that there is good correlation between the present experimental results and those in the literature [4]. Note that the friction factor is obtained from the Darcy friction factor normalized by the number of rows of the pin fin array, the friction due to the test section is subtracted and only the friction contribution due to the pin fins is accounted. It can be seen that as the Reynolds number increases the friction factor decreases for the case studied, in agreement with Gunter and Shaw [26]. Due to the high energy of the flow at higher Re the fluid is able to pass through the cavity with a decreased separation at the pin fins and it is well know that as the Re increases the friction factor in a duct flow decreases [18]. These two factors contribute to the overall friction factor decrease even though the friction due to the channel is not taken into account.

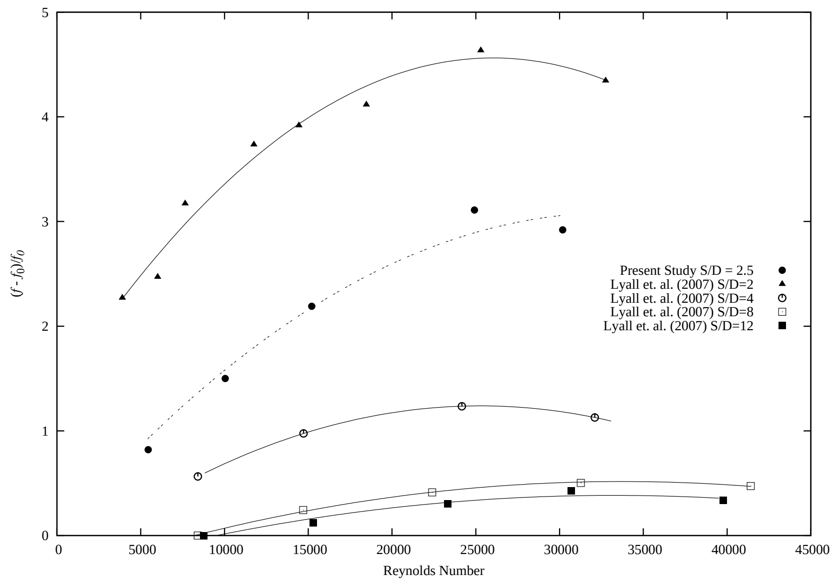

Figure 5–2: Present study experimental friction factor augmentation compared with the results obtained by Lyall et. al. [3]

Lyall et. al. [3] compute the friction factor augmentation by assuming a baseline friction factor (f_0) of an empty channel of the same test section length and comparing it to the actual friction factor of one row of pin fins. The baseline friction factor used by [3] is:

$$f_0 = 0.5072Re^{-0.3} \tag{5.5}$$

This method allow us understand how much the friction factor is increased due to the blockage formed by one row of pin fins when compared to the empty channel. By using the same method of [3] it can be shown in figure 5–2 that for one row of pin fins the friction factor augmentation increases as the Reynolds number increases (the same trend as [3]). Lyall et. al. [3] does not present a case of $\frac{S}{D} = 2.5$ instead they have a case of $\frac{S}{D} = 2$ and 4. The present results are in good agreement with [3] since they fit between the $\frac{S}{D} = 2$ and 4 lines and it is more close to the $\frac{S}{D} = 2$ values.

Figure 7–9 shows the present results for the friction factor obtained experimentally. The results are plotted in a per row basis for the cases studied. They show that for one and two rows of pin fins the friction factor tends to increase as the

Reynolds number increases. This behavior is expected since the rows add a blockage to the flow in the test section increasing the overall friction factor. In case of the two rows array the wake of the first row is interrupted by the second row creating a greater disturbance of the flow. When the array have three rows the friction factor is in a transition since it first increases, then reaches a maximum, and finally decreases as the Reynolds number increases. For four up to ten rows the friction factor tends to decrease with the increase of the Reynolds number, but it is from six to ten rows that we have the same decreasing behavior of the friction factor. The fact that the friction factor decreases as the Reynolds number increases is because the firsts four rows absorbs the flow energy decreasing the effect of adding another row to the array. With more rows in the pin fin array the flow develops becoming more symmetric in the downstream rows. From the results it can be concluded that when the number of rows is greater than six the friction factor will always decrease with an increase in the Re.

Total pressure drop in the test section is compared to the pressure difference created by the pin fin array itself. The total pressure difference (ΔP_{Total}) represent the flow energy loss due to the skin friction of the channel and the pin fins and the form drag of the pin fins. On the other hand the pressure drop due to the array (ΔP_{Array}) is the energy loss created by the pin fins only in the test section it also contains the skin friction drag and the form drag. The ratio of these two values is taken as a measurement of the contribution of the pin fins and the plain channel to the total pressure drop in the test section. Figure 5–4 shows the ratio between these two values as a function of the number of rows and the Re. The figure shows that as the number of rows increases the ratio becomes steady and losses its dependency on the Re. This shows that for more than six rows the contribution of the channel to the pressure drop becomes less than 10% and the pin fin array contributes the other 90% no matter the Re.

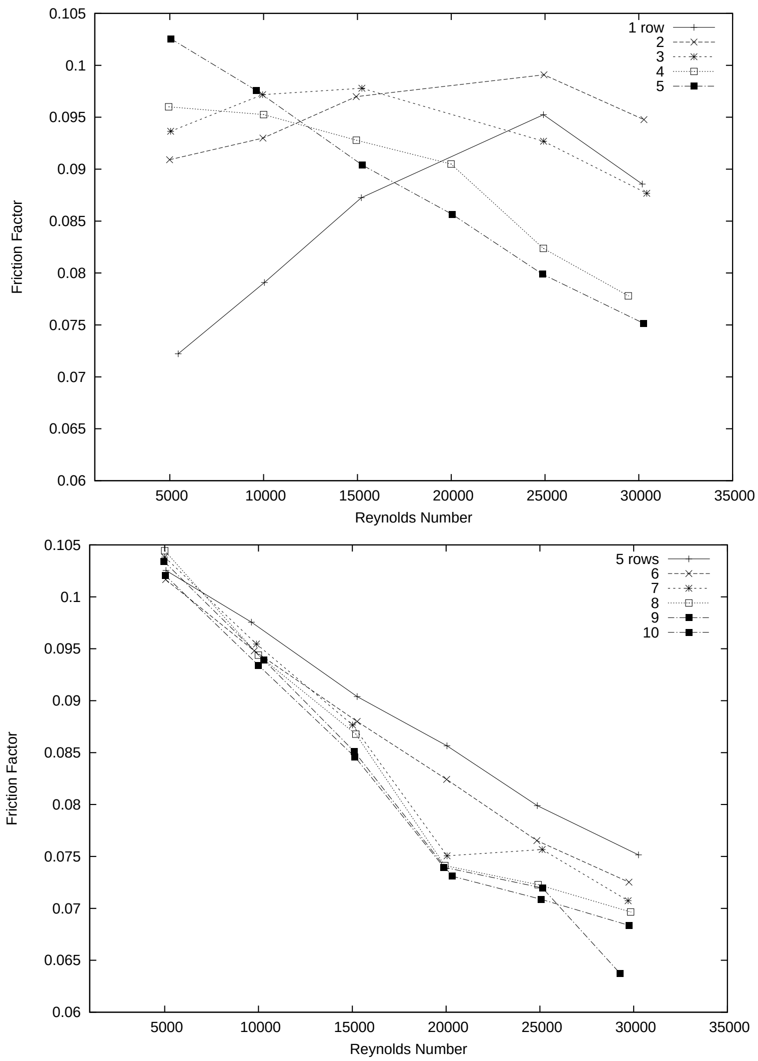

Figure 5–3: Friction factor for different arrays of pin fins. The spanwise distance ratio ($\frac{X}{D}$) is set to 1.5 and $\frac{S}{D} = 2.5$.

5.3 Concluding Remarks

Experiments show good agreement with literature (Fig. 7–12), from them it can be concluded that the effect of the addition of one more row affects the overall friction factor on the channel (Fig. 7–9). For more than two rows the tendency of the friction factor is to increases as the Re increases. For three rows f starts to increase and then decrease as the Re increases. Finally, for more than four rows on the array f decreases when the Re increases. The pressure drop due to the array of pin fins in the test section represents more than 90% for more than six rows, the

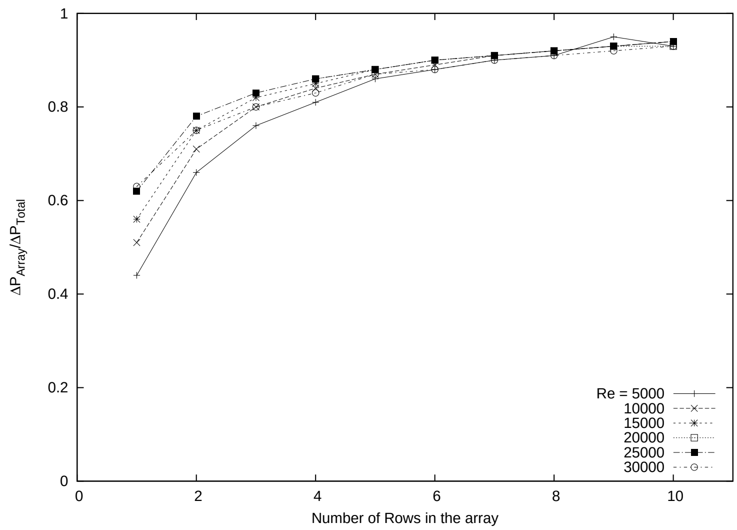

Figure 5–4: Pressure difference across the channel due to the pin fin array normalized by the total pressure drop in the test section for difference Re and number of rows.

other 10% is due to the channel friction losses and it is independent of the Re (Fig. 5–4).

Present experimental findings on the friction factor and the pressure contribution of the array to the total pressure loss serve as a valid base for the periodic boundary conditions on the numerical experiments. The periodic boundary conditions are indeed an infinite number of rows and experiments prove that for more than six rows the studied passive scalars does not varies significantly. Next chapters will take into consideration this fact as a standpoint to study the effect of the streamwise spacing, the spanwise spacing and the effect of the Re on the friction factor and the heat transfer.

CHAPTER 6
EFFECT OF STREAMWISE SPACING ON PIN FINS HEAT TRANSFER AND FRICTION FACTOR

6.1 Numerical Results and Discussion

Numerical results were also validated with the experiments as shown in figure 7–12. Note that the friction factor obtained by numerical simulations correlates very well with the Metzger et. al. [4] correlation for lower Reynolds numbers, even that the channel used is periodic in the spanwise and the streamwise directions. This is true since the contribution of the sidewalls of the test section is negligible. From experiments it can be concluded that as the number of pin fins rows is more than six the friction factor present the same behavior [36], and therefore this allow us to compare an infinite number of rows from the DNS periodic conditions to the experimental measurements for ten rows of [4].

The effect of the streamwise spacing was observed by selecting a constant Reynolds number of 4000 and in the case of the streamwise variation the distance to diameter ratio ($\frac{S}{D}$) was set equal to 2.5 and the streamwise distance was varied as $1.5 < \frac{X}{D} < 6$. The turbulent heat flux is taken at $0.1D$ in the normal direction from the hot wall and it is averaged in time and space and divided by the area of the computational box minus the cross sectional area of the pin fins, which gives the heat transfer area. Metzger et. al. [4, 17] states that the heat transfer is affected by the spacing between the pin fins, indeed they found that for closer pin fin spacing the heat transfer was higher. The effect of changing the spacing in the flow and the heat transfer will be reviewed by its effect on the mean flow, on the turbulence, the heat transfer, and friction factor.

6.1.1 Mean Flow

Color contours time averaged streamwise velocity for $Re = 4000$ are shown in figure 7–1, at $0.1D$ from the hot wall. The contours depicts the behavior of the velocity with the variation of the streamwise spacing. The flow behavior around the pin fins resembles the flow around an infinite cylinder, but in these cases the wake length (Fig. 7–3) and the pressure gradient is affected by the near pin fins and the end wall interaction. When the flow reaches the pin fin there is stagnation of the fluid at the leading edge, as it moves through the circumference the flow accelerates and increases its velocity. Finally the boundary layer separates from the body, due to the adverse pressure gradient. Behind the pin fin there is a wake formation that extends for a certain distance L depending on the spacing. Results shows that the wake length (L) at the mid plane increases as the streamwise distance between the rows increases.

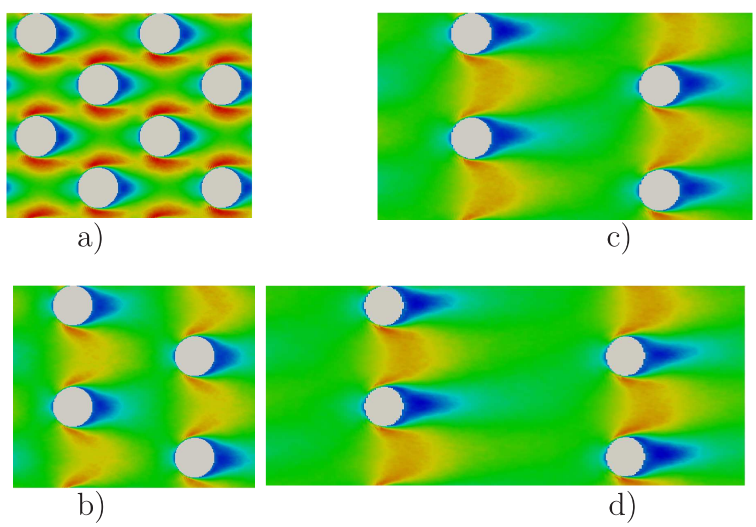

Figure 6–1: Time averaged streamwise velocity color contours for $Re = 4000$ of the four cases studied at $0.1D$ from the hot wall. The streamwise distance for the cases are: a) $\frac{X}{D} = 1.5$, b) 3, c) 4.5, and d) 6. Red means high and blue means low velocity.

The configuration with $\frac{X}{D} = 1.5$ has the larger density of pin fins and it presents the highest velocity in the streamwise direction (fig. 7–1 a). Velocity increases on the side of the pin due to the conservation of mass, in fact, the pin are a blockage to the flow which is forced to pass through a smaller area. A street of high velocities can be observed on the side of the pins. A small velocity region occurs in the wake of the pin. By increasing the streamwise distance of the array ($\frac{X}{D}$) the interference between the consecutive rows becomes weaker. The streaks of high velocity observed for $\frac{X}{D} = 1.5$ disappear. The increase of the velocity on the side of the and the low velocity behind the cylinder are confined to a smaller area.

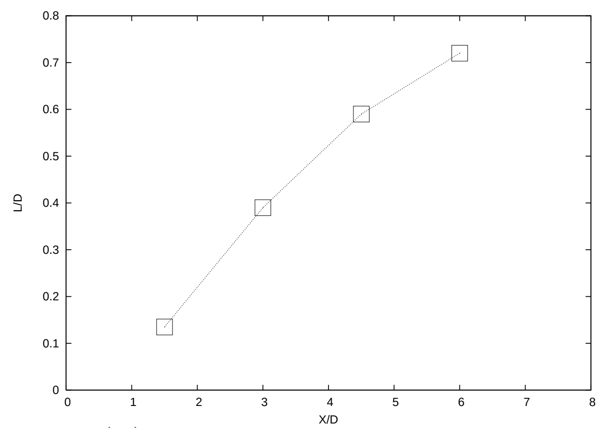

Figure 6–2: Wake length (L) dependence on row streamwise distance $\left(\frac{X}{D}\right)$ for Re = 4000 at the mid plane of the channel. The wake length is normalized by the diameter of the pin fin D.

The wake behind length was measured for the 4 different cases considered. For small $\frac{X}{D}$ the wake is shortened by the following row of the pin. By increasing the $\frac{X}{D}$ the length of the wake becomes close to the wake of an infinite cylinder. The wake in this two cases is larger than in the smaller spacing cases (Fig. 7–3). This means that for the smaller spacing cases the adjacent rows are breaking the wake behind the pin fin.

Figure 6–3 shows a side view in a plane that passes through the center of a pin fin. In the near wall regions the length of the wake is larger. This effect is augmented by increasing the distance between the consecutive rows ($\frac{X}{D}$). As the flow moves downstream it accelerates before reaching the next row, this is due to the high velocity zones between the pin fins on the same row (Fig. 7–1).

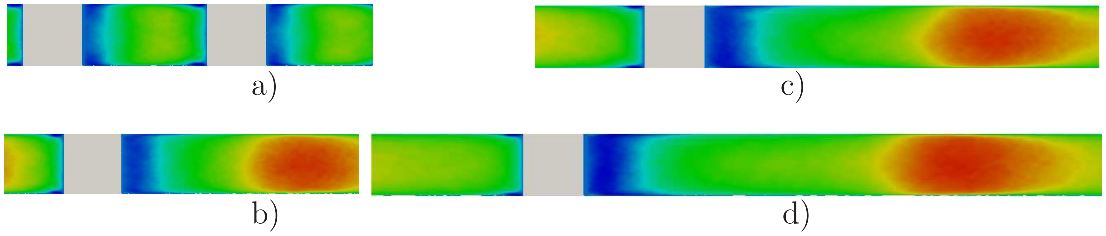

Figure 6–3: Time averaged streamwise velocity color contours for $Re = 4000$ of the four cases studied at $0.1D$ from the hot wall. The streamwise distance for the cases are: a) $\frac{X}{D} = 1.5$, b) 3, c) 4.5, and d) 6. Red means high and blue means low velocity.

The time average is a good approach to obtain a steady state results, but it is known that the wake behind a cylinder oscillates and the vortex detaches from the body. These features will have an effect on the flow and the heat transfer behavior for the different cases. In the next section instantaneous visualizations are shown.

6.1.2 Instantaneous Visualizations

Instantaneous streamwise velocity visualizations in a plane at $0.1D$ from the hot wall (Fig. 6–4) show the unsteady behavior of the flow. The wake behind the pin fins shed and it also produces alternating eddies that detaches from the pin fin (Fig. 6–4 c). Localized high velocity regions can be seen in fig. 6–4a), this regions affect the stagnation point of the pin fins at the next row by displacing it in a certain direction opposite to the high velocity region. This localized velocity affect the instantaneous heat transfer and can be a possible source of material creep due to the temperature difference that the forced convection will cause. For $\frac{X}{D} = 3$ (fig. 6–4b) shows that the wake is interrupted by the next staggered row. This means that the incoming flow for the next row is affected by the upstream pin fins causing differences in the heat transfer around the pin fin and the endwall. Since the wakes are reaching the next rows of pin, the flow is more likely to be disturbed and the mixing and heat transfer is enhanced by this feature.

For larger $\frac{X}{D}$ (>3), the wake region dissipates before reaching the next row, therefore more a uniform flow reaches the next row (fig. 6–4 c, d). Due to the nature of the channel the vortex that detaches from the pin fins rapidly dissipates

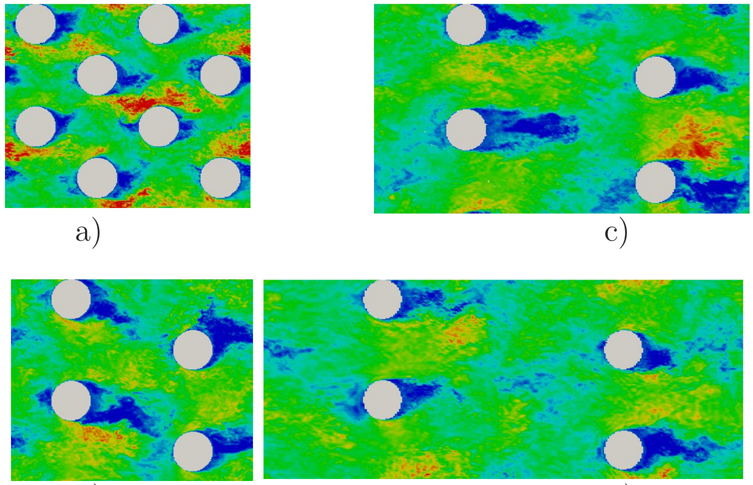

a) c)

b) d)

Figure 6–4: Instantaneous streamwise velocity color contours for $Re = 4000$ of the four cases studied at $0.1D$ from the hot wall. The streamwise distance for the cases are: a) $\frac{X}{D} = 1.5$, b) 3, c) 4.5, and d) 6. Red means high and blue means low velocity.

reducing the mixing of the flow. This cases also show localized regions of high velocity near the pin fins surfaces where the pressure gradient is favorable and wake shedding at the pin fin trailing edge. The figure shows an nonparallel shedding between the pin fins meaning that the shedding is occurring in different periods for the same time unit and the same flow conditions.

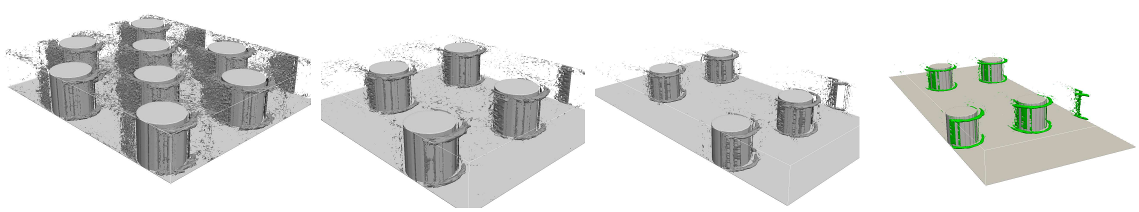

a) b) c) d)

Figure 6–5: Horseshoe vortex formation in the cylinder endwall interface zones for $Re = 4000$ and cases $\frac{X}{D} = 1.5$ a), 3 b), 4.5 c), and 6 d).

Endwall effects play an important role in the development of the wakes, the vortex stretching and the heat transfer in the array. Turbulent structures, like horseshoe vortices, are promoted in the interface between the pin fin and the end-wall [16]. They are responsible for the augmentation of the heat transfer in the hot wall since they move the fluid cold layers near the hot wall. Visualizations of average vortical structures (Fig. 6–5) shows the formation of the horseshoe vortex in the endwall-pin fin interface. As the space between the rows is decreased the vorticity becomes more complicated and isotropic. The method used to identify these structures in figure 6–5 was the λ_2 criterion developed by Jeong and Hussain [37]. This method first take the gradient of the Navier-Stokes equations and decompose it into the symmetric and antisymmetric parts (vorticity transport equation), S^2 and Ω^2 respectively. They use $S^2 + \Omega^2$ to determine a local pressure minimum due to the vortical motion and two negative eigenvalues of $S^2 + \Omega^2$ in a continuous region as a definition of a vortex core. With these definitions $\lambda_2 < 0$ at a vortex core, been λ_2 the second eigenvalue of $S^2 + \Omega^2$. This method is more effective when studding evolutionary dynamics and flow features of vortices [37]. The strain and rotation tensor where built with the time average flow field and a value of $\lambda_2 =$ -1 was selected for the isosurfaces in figure 6–5.

Heat transfer in the array is mainly accomplished by convection due to the turbulence generated in the array. Figure 7–8 shows the average turbulent heat flux at $0.1D$ from the hot wall to the cold wall. Pin fin heat addition is accounted in the turbulent heat flux since the only way the heat can exit is through the cold wall. From this figure it can be shown that the heat transfer increases as the row distance decreases. Figure 7–8 a) shows an increased turbulent heat flux, but it has zones at the leading edges of the pin fins where the heat flux is negative meaning that the heat is transported toward the hot wall, this affects the average heat transfer in the study plane. This case shows a higher turbulent heat flux at the zone between the pin fins. The average heat transfer will be discussed in the next section.

For $\frac{X}{D} = 3$ the turbulent heat flux larger than that for $\frac{X}{D} = 4.5$ because of the interaction between the downstream rows. The proximity of the rows and the interaction between the wake and the next row (fig. 6–4) causes an increase in the heat transfer in the section. For large $\frac{X}{D}$ (> 3) the turbulent heat flux approximates

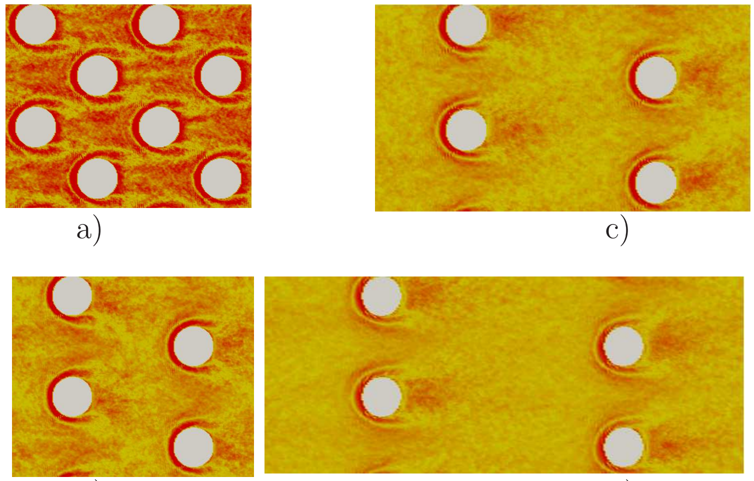

a) c)

b) d)

Figure 6–6: Time averaged turbulent heat flux <Tv> color contours for $Re = 4000$ of the four cases studied at $0.1D$ from the hot wall. The streamwise distance for the cases are: a) $\frac{X}{D} = 1.5$, b) 3, c) 4.5, and d) 6. Yellow means low and red means high <Tv>.

to zero (yellow) in the region between the rows. This is because the flow starts to develop and turbulence is dissipated (Fig. 7–1). In all cases the zone that present an increased heat transfer (red) is the zone between the pin fins in the spanwise direction where the velocity increases and at the trailing edge of each pin fin. There are also common zones of increased heat transfer at the leading edge of each pin fin that extends to the separation point of the boundary layer.

6.1.3 Heat Transfer and Friction Factor

Figure 6–7 shows time averaged turbulent heat flux (<Tv>) per unit area at $0.1D$ from the hot wall. The results show that there is a streamwise spacing where the turbulent heat flux per unit area is maximized. By reducing the distance between consecutive rows, i. e. the case of $\frac{X}{D} = 1.5$, the pin fins create a blockage for the flow and forces the fluid to pass only through the space between the pins. This induces an increase in the velocity in the area between the pin fins and a sudden reduction caused by the next row. Since the $\frac{X}{D}$ is small the disturbance has not enough space to be dissipated, making the vorticity more intense and therefore increasing the heat transfer. It must be acknowledged that the heat transfer per unit area for this configuration is higher than cases with larger configurations.

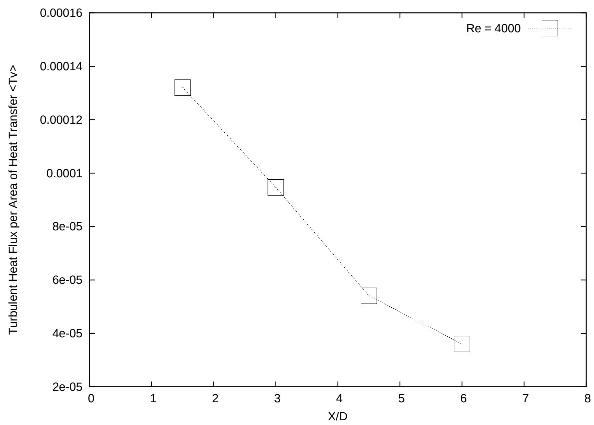

Figure 6–7: Dependence of the turbulent heat flux per unit area for $Re = 4000$ as the streamwise distance is varied in the range of $1.5 < \frac{X}{D} < 6$.

It was found that the convective heat transfer per unit area is reduced by 33% at $\frac{X}{D} = 3$ when compared to $\frac{X}{D} = 1.5$. This configuration promotes the generation of turbulent structures that enhances the mixing between the cold fluid in the upper layers and the hot fluid in the near wall region. The space between the rows is enough for the flow to remove a great amount of heat from the hot wall before encountering the next row where it is disturbed again. At a greater streamwise spacing the pin fins start to act more independently and the advantages of the array is lost since there is no interaction of the flow disturbances between the adjacent rows. The flow starts to develop as well as the thermal boundary layer in the area between the rows and the turbulent structures dissipate before they reach the next row reducing the amount of heat removed per unit area by more than 54.6%.

Pin fins augment the heat transfer on the endwalls due to the flow disturbances created at the leading edge of the cylinder and the wake behind it. The Nusselt number (Nu) represents the ratio between the convective heat transfer to the conductive heat transfer from the endwall surface to the fluid [19]. In its dimmensionless form the Nu is represented as:

$$Nu = \left(\frac{\partial T}{\partial y}\right)_{y=0} \tag{6.1}$$

where $\frac{\partial T}{\partial y}$ is the temperature gradient at the surface [19]. The spacing between the pin fins affect this transfer quantity (fig 6–8). As the streamwise space increases the Nu decreases as the same as experiments [5, 16]. The decrease in the Nu with the larger spacings is due to the dissipation of the disturbaces and the developing boundary layer which decreases the heat transfer (see fig. 7–8).

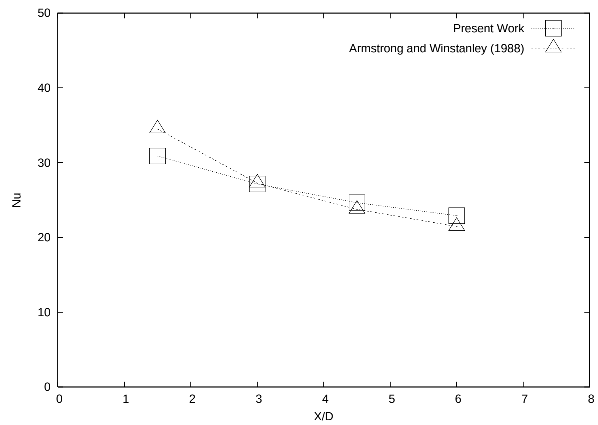

Figure 6–8: Dependence of the endwall Nusselt number for $Re = 4000$ as the streamwise distance is varied in the range of $1.5 < \frac{X}{D} < 6$ compared with Armstrong and Winstanley [5] (experimental).

The flow features created by the pin fin-endwall interface increases the heat transfer when compared with the plain duct flow. The plain duct or base line Nu used in this work is the same used by Lyall et. al. [3] and it is defined as:

$$Nu_0 = 0.022Re^{0.8}Pr^{0.5} \tag{6.2}$$

The augmentation of the Nu accounts for the extra heat transfer added by the pin fins. This augmentation $\left(\frac{Nu}{Nu_0}\right)$ is affected by the streamwise distance of the pin fins as shown on figure 6–9. As the streamwise space is increases the augmentation of the heat transfer decreases. This means that as the streamwise space increases the plain duct heat transfer dominates and the disturbaces effects are less effective.

The friction factor (f) is the parameter that represent the resistance of the flow in the cavity with the pin fins. Since the flow is forced by a pressure gradient through the channel it must take in to account the friction skin drag and the form

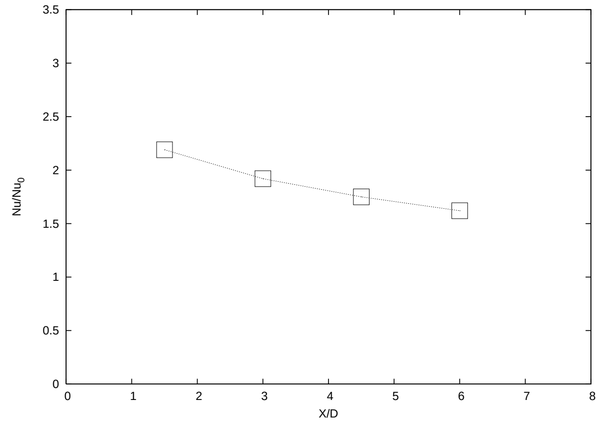

Figure 6–9: Dependence of the Nusselt number augmentation for $Re = 4000$ as the streamwise distance is varied in the range of $1.5 < \frac{X}{D} < 6$

drag. The force needed to make the fluid flow represents the compressor work needed to cool down the blade, therefore the less drag the better in terms of overall engine efficiency. The friction factor was computed as follows:

$$f = \frac{2\Delta\tilde{P}}{\rho V_{max}^2 N} \tag{6.3}$$

where $\Delta\tilde{P}$ is the pressure gradient needed to maintain a constant flow rate, i. e. Π, ρ is the fluid density, V_{max}^2 is the average maximum velocity, and N is the number of rows.

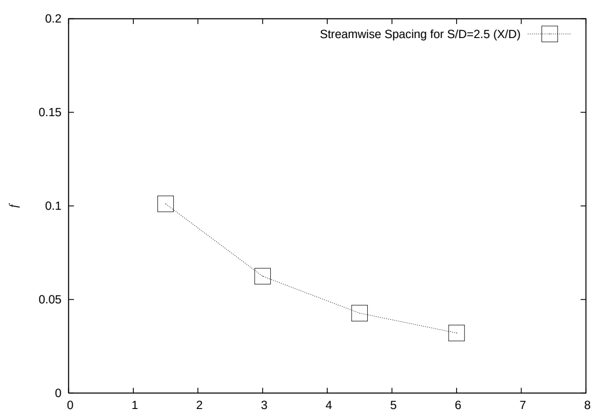

Figure 6–10: Dependence of the friction factor on $\frac{X}{D}$ and $Re = 4000$.

Figure 6–10 shows the friction factor normalized by the number of rows for each streamwise spacing configuration. It shows that as the space is increased between the rows less drag in the array is generated. In a previous paper Cruz Perez et. al.

[36] found that approximately 90% of the drag generated is due to the form drag. This means that the reduction in the overall friction factor is mainly due to the form drag generated by the pin fins. The trend shown in figure 6–10 shows that as the distance of the rows increases the friction factor will converge to a single row case. A single row case is not practical since the pin fin array provides structural support to the blade trailing edge.

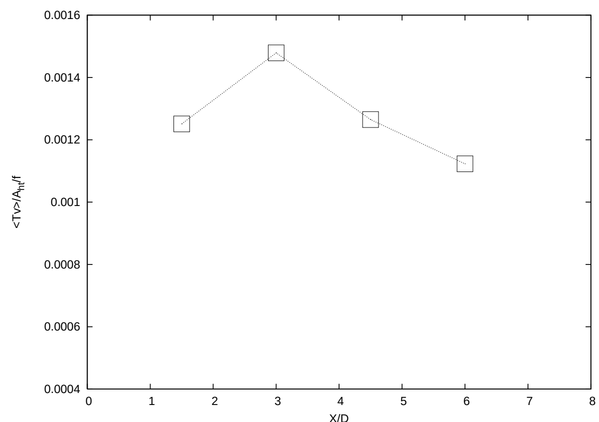

Figure 6–11: Heat transfer to friction factor ratio for the $\frac{X}{D}$ studied and $Re = 4000$.

The most efficient configuration is the one that maximizes the ratio between the heat transfer and the friction factor ($\frac{Tv/A_{ht}}{f}$). Figure 6–11 shows the variation of this ratio with the streamwise distance. It shows that there is an increase in the ratio, reaches a maximum and decrease smoothly. Based on this ratio the streamwise spacing that provides the maximum heat transfer with the less pressure drop possible is $\frac{X}{D} = 3$.

6.2 Concluding Remarks

The mean flow through the array shows an increase in the velocity in the region between the pins and a decrease before reaching the next row. The wake behind the pins becomes larger as the streamwise distance of the row increases. The instantaneous flow is characterized by localized high velocity zones, oscillations of the wake behind the pins and wake interaction with the adjacent row. Larger spacing shows dissipation of the wake and the detached eddies. Vorticity becomes higher and more isotropic as the row distance decrease therefore increasing the heat transfer.

Pin fins arrays enhance the heat transfer in a channel by promoting turbulent structures in the endwall-pin fin interface. These structures improve the mixing by moving the cold fluid layers near the hot wall. The interaction between the structures of the nearby pin fins increases the turbulence and therefore the overall heat transfer in the array. It was found that the smaller row space, $\frac{X}{D} = 1.5$, provides the highest heat transfer per unit area. This configuration augments the heat transfer 2.19 times more than the plain channel.

By closing the row distance, it was found that the heat transfer increases in the array in a per unit area basis. The trade-off of closing the space between the rows is the augmentation of the friction factor. The friction factor represents the work that is required to maintain a constant flow rate through the array. The most efficient configuration is the one that increases the ratio between the heat transfer and the friction factor, which is $\frac{X}{D} = 3$.

CHAPTER 7
EFFECT OF SPANWISE SPACING AND REYNOLDS NUMBER ON PIN FINS HEAT TRANSFER AND FRICTION FACTOR

7.1 Numerical Results and Discussion

The effect of the spanwise spacing was tested by setting a constant streamwise distance of $\frac{X}{D}$ of 3 and the $Re = 4000$, this streamwise spacing showed a better performance for constant spanwise distance as shown in the previous chapter. The spanwise distance was varied between $1.5 < \frac{S}{D} < 6$ and the turbulent heat flux is averaged at $0.1D$ in the normal direction from the hot wall and it is averaged in time and space. Nusselt number was taken at the surface and it was compared with the Nu of the plain duct using the correlation used by Lyall et. al. [3]. In the cases where the Re was varied the geometry was set to a spacing of $\frac{X}{D} = 1.5$ and $\frac{S}{D} = 2.5$ which is the same configuration used for experiments and the same factors were accounted to understand the effect of the Re on the array.

7.1.1 Mean Flow

Velocity color contours of time averaged streamwise velocity (fig. 7–1) shows that as the spanwise space between the pin fins is increased the maximum average velocity decreases. For the cases with smaller space between the pins it is found an increase in the velocity in the zone between the pins of the same row to maintain a constant flow rate. It was observed for case of $\frac{S}{D} = 1.5$ a jet like flow in the zone between the pin fins of the same row. This jet like feature increases the local velocity thus inducing a longer wake. The increased velocity is then rapidly decreased by the blockage created by the next row of the array. The effect of blockage is seen as the green zone (Fig. 7–1) in the space between the rows and the stagnation zone at the leading edge of the pin fins. The blockage becomes ineffective as the $\frac{S}{D}$ is increased. As the infinite cylinder, there is a stagnation point at the leading edge of the pin fins and a wake behind each pin. The wake becomes larger as the spanwise distance is increased, this is because for larger spacings less fluid particles moves in the spanwise direction since they have enough space between the pins to pass without a significant resistance.

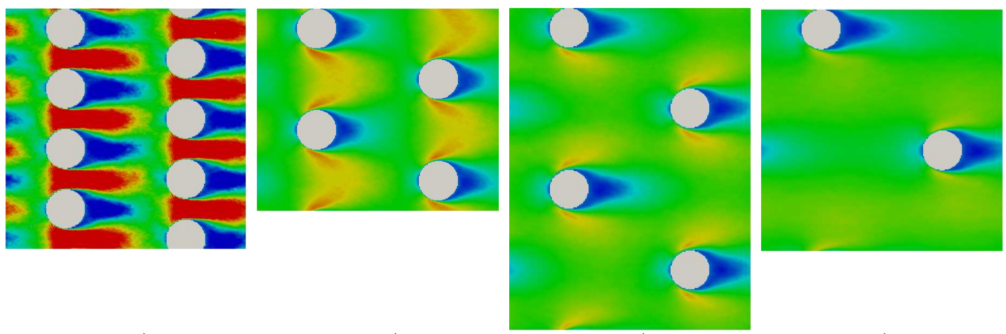

a) b) c) d)

Figure 7–1: Time averaged streamwise velocity color contours for $Re = 4000$ of the four cases studied at $0.1D$ from the hot wall. The spanwise distance for the cases are: a) $\frac{S}{D} = 1.5$, b) 2.5, c) 4, and d) 6. Red means high and blue means low velocity.

Reynolds number plays an important role in the array heat transfer and friction factor. The velocity field is also affected by this dimensionless number. Figure 7–2 show a time averaged streamwise velocity color contour of the same geometrical configuration $\frac{S}{D} = 2.5$ and $\frac{X}{D} = 1.5$. As the Re is increased the mean velocity also increases at the region between the pins, this can be noted in the bigger red zones at the favorable pressure gradient zone that goes from the leading edge to approximately 82 deg. in figure 7–2. The bigger red zones are because separation at the surface of the cylinders is delayed and the wake behind the pin fins is longer. Peng [12] found that closely spaced configurations forces the flow through the streamwise space available between the pin fins, same as seen in figure 7–2.

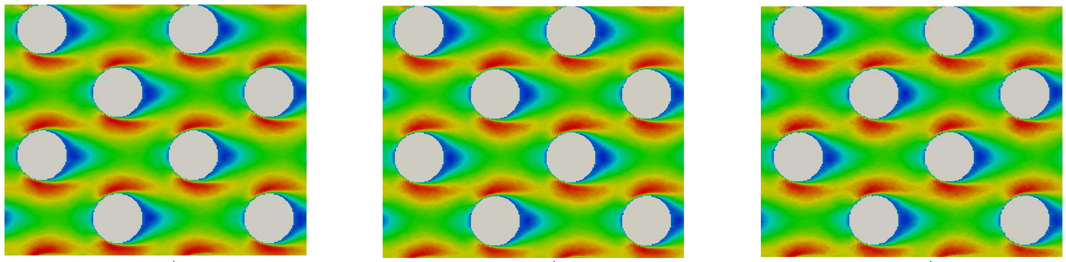

a) b) c)

Figure 7–2: Time averaged streamwise velocity color contours at $0.1D$ from the hot wall for $\frac{S}{D} = 2.5$ and $\frac{X}{D} = 1.5$. The Re is 2000 for a), 4000 for b), and 6000 for c). Red means high and blue means low velocity.

Figure 7–3 a) shows the average wake length in terms of the diameter for each case at the mid plane. It shows that the wake augments its length as the spanwise distance increase, except for case $\frac{S}{D} = 1.5$ where the wake is longer due to the jet like flow between the pin fins of the same row. The increase in the wake length for the larger spacings is because the fluid is more free to pass between the rows. As it can be seen from figure 7–1 the interference between the pin fins is reduced, this allow the wake to form without any obstruction. On the other hand, figure 7–3 b) shows that as the Re is increased for a closed spacing array the wake length decreases. This wake behavior is important because many of the heat transfer and flow disturbance occurs at the wake behind the pin fins. The wake length is reduced with higher Re because the fluid that impinges on the pin is forced flow to the sides and this forces the wake to be smaller and increases the velocity in the region between the rows.

7.1.2 Instantaneous Visualizations

Instantaneous visualizations of the streamwise velocity at a plane at $0.1D$ from the hot wall shows the interaction between the disturbed flow from the upstream row and the subsequent row. Instantaneous high velocity zones are observed for $\frac{S}{D} = 1.5$ at any position of the wake during the shedding since the spanwise space is limited through the pin fins and the high velocity is more due to constant flow rate than to the flow shedding. For $\frac{S}{D} = 1.5$ and 2.5 the wake of the pin interacts with the downstream pin, shifting the stagnation point of the pin fin. This instantaneous

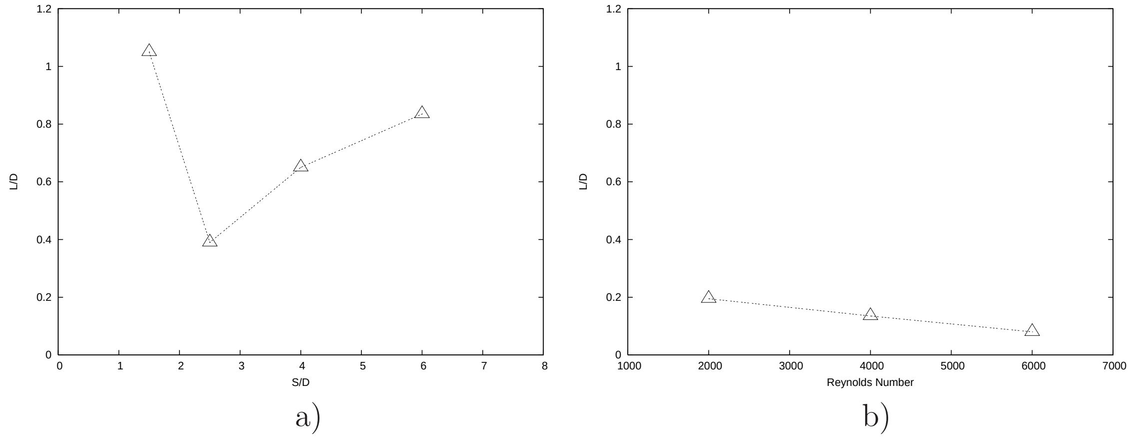

Figure 7–3: (a) Wake length (L) dependence on the spanwise distance $\left(\frac{S}{D}\right)$ for Re = 4000 at the mid plane of the channel. (b) L dependence on Re for $\frac{S}{D} = 2.5$ and $\frac{X}{D} = 1.5$. The wake length is normalized by the diameter of the pin fin D.

interaction changes the favorable pressure gradient of this cylinder and therefore affects the boundary layer separation and the trailing edge wake of the pin fin. As the spanwise spacing is increased the interaction between the wake and the stagnation point of the next rows is loss and the fluid flows more freely through the array.

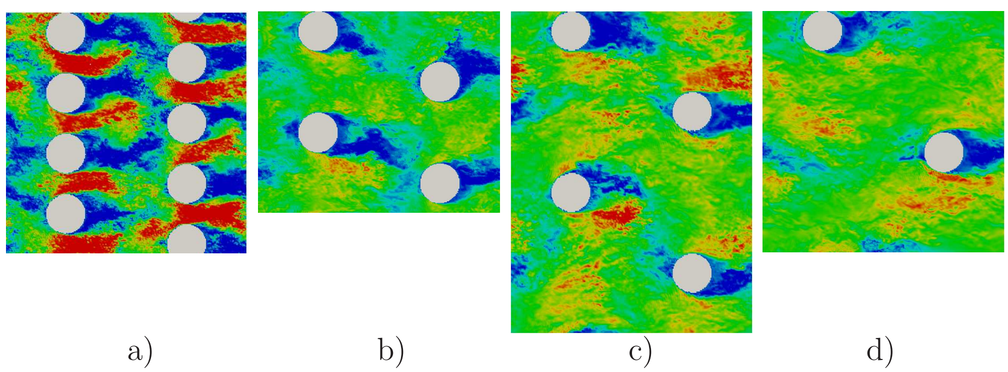

Figure 7–4: Instantaneous streamwise velocity color contours for $Re = 4000$ of the four cases studied at $0.1D$ from the hot wall. The spanwise distance for the cases are: a) $\frac{S}{D} = 1.5$, b) 2.5, c) 4, and d) 6. Red means high and blue means low velocity.

As the Re is increased for the same spacing conditions localized high velocity zones at the side of the pin fins circumference becomes larger (fig 7–5). This effect is not clear for $Re = 4000$ due to the oscillations of the flow at that time through the cavity (fig 7–5 b). When the wakes are aligned during the shedding localized high velocity zones disappear since the fluid is not forced by the wakes to flow through the opposite side of the pin fin wake. Figure 7–5 a) and b) shows the formation of a high velocity zone due to a wake shedding. For conservation of mass the fluid must skip this low velocity zones and therefore increases its velocity in the opposite side of the wake.

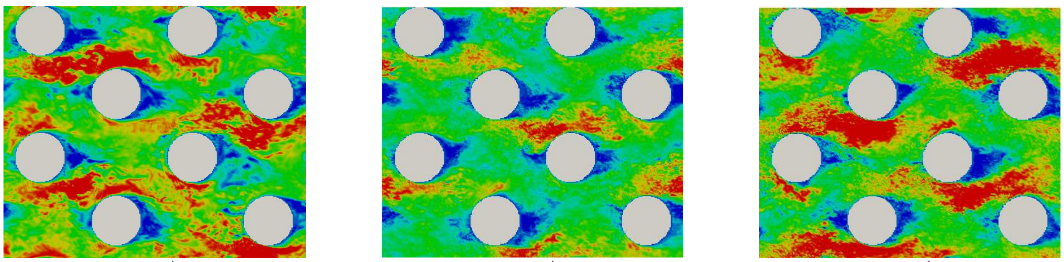

a) b) c)

Figure 7–5: Time averaged streamwise velocity color contours for $\frac{S}{D} = 2.5$ and $\frac{X}{D} = 1.5$. The Re is 2000 for a), 4000 for b), and 6000 for c). Red means high and blue means low velocity.

Non-steady conditions in the flow promotes the convective heat transfer in the array. Figure 7–6 shows the time averaged heat flux at $0.1D$ from the hot wall. This figure shows that the heat flux increases as the spanwise space between the pin fin is reduced. Case $\frac{S}{D} = 1.5$ shows (fig. 7–6 a) more heat transfer due to the disturbaces created by the jet like flow when it impignes on the next downstream row. In the case of $\frac{S}{D} = 2.5$ (fig. 7–6 b) there is major zone of heat transfer between the pin fins of the same row. As the S is increased ($\frac{S}{D} > 2.5$) the interaction of the nearby pin fins is lost and the pin fins behave as separate heat transfer promoters. For the larger spacing cases the heat transfer occurs mainly at the leading edge of the pin fins and at the wake region behind the pin. Since there is no wake interaction with the downstream rows the heat transfer of the next row is not affected by the flow disturbances of the wake (fig. 7–6 b).

Reynolds number also have an effect on the heat flux of the array (fig. 7–7). As the Re increases the heat flux decreases for the same spacing configuration. Since the fluid is forced to flow through the available space between the adjacent pin fins the heat transfer in the zone between the rows is reduced. These cases demonstrate

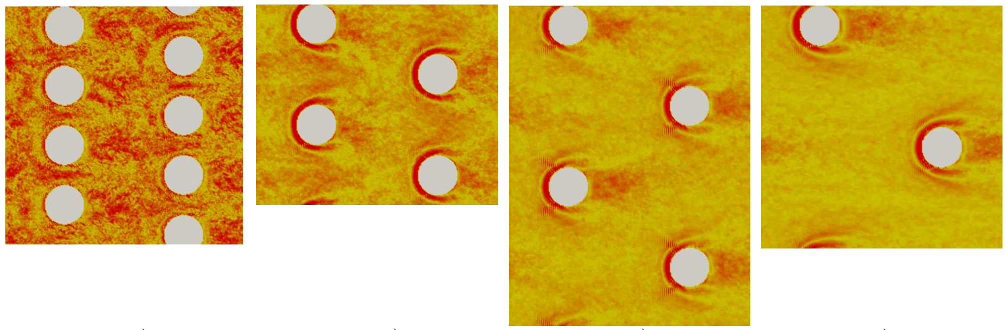

a) b) c) d)

Figure 7–6: Time averaged turbulent heat flux $< Tv >$ color contours for $Re = 4000$ of the four cases studied at $0.1D$ from the hot wall. The spanwise distance for the cases are: a) $\frac{S}{D} = 1.5$, b) 3, c) 4, and d) 6. Red means high and yellow means low turbulent heat flux.

that the wake length plays an important role in the heat transfer. As the wake length is reduced due to the flow conditions (fig. 7–3 b)) the heat transfer is also reduced. The wake is responsible for some of the augmentation of the heat transfer, but in these cases, with short space between the pins, the wake is not able to develop in an optimum fashion. The high velocity zones (fig. 7–2) also disturbs the wake development resulting in less turbulent flux per unit area as the Re increases.

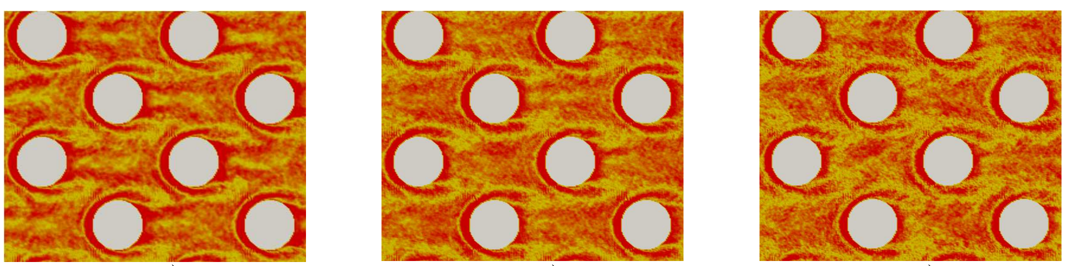

a) b) c)

Figure 7–7: Time averaged turbulent heat flux $< Tv >$ color contours for $\frac{S}{D} = 2.5$ and $\frac{X}{D} = 1.5$. The Re is 2000 for a), 4000 for b), and 6000 for c). Red means high and blue means low velocity.

7.1.3 Heat Transfer and Friction Factor

The spanwise space affects the heat transfer by increasing it with the smaller spacings, this agrees with [16, 17]. From figure 7–8 a) it can be shown that the average turbulent heat flux per unit area decreases as the spanwise distance ($\frac{S}{D}$) increases. This reduction in the heat transfer is due to the loss of interaction of the adjacent pin fins as can be seen in figure 7–1 and 7–6. The average turbulent heat flux per unit area for cases $\frac{S}{D} = 4$ and 6 is almost similar since all interaction between nearby pin fins is loss. For these two cases the friction factor, the structural stability and/or manufacturing constraints will dictate the eligibility of these two configurations.

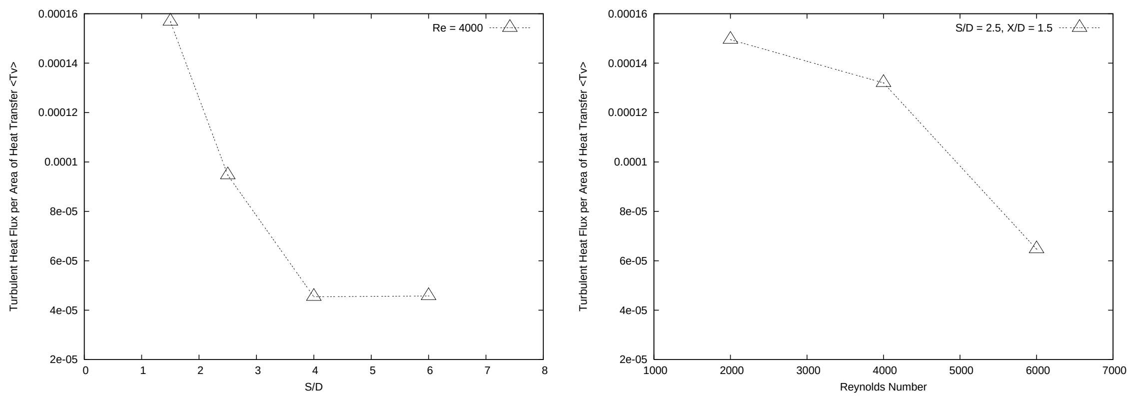

a) b)

Figure 7–8: (a) Dependence of the turbulent heat flux per unit area of heat transfer on $\frac{S}{D} = 2.5$ for $Re = 4000$. (b)Dependence of the turbulent heat flux per unit area of heat transfer on Re for $\frac{S}{D} = 2.5$ and $\frac{X}{D} = 1.5$.

The average heat flux per unit area decreases as the Re increases for the same configuration (fig. 7–8 b)), which is the same trend obtained by [12, 38]. They use the Colburn j-factor as the heat transfer coefficient for the arrays and it is defined as:

$$j = St_{HT} Pr^{\frac{2}{3}} \tag{7.1}$$

where j is the Colburn j-factor and St_{HT} is the Stanton number [19] (the subscript HT is used to differentiate the Stanton number from the Strouhal number from Chapter 2). The decrease in the average turbulent heat flux is due to the reduced wake formation at the trailing edge of the cylinders due to the endwall effects. The reduction in the heat transfer is contrary to the infinite cylinder and the long cylinder arrays which increase the heat transfer as the Re is increased [19]. This demonstrate that the endwalls play an important role on the heat transfer of the pin fin array in agreement with [17, 33].

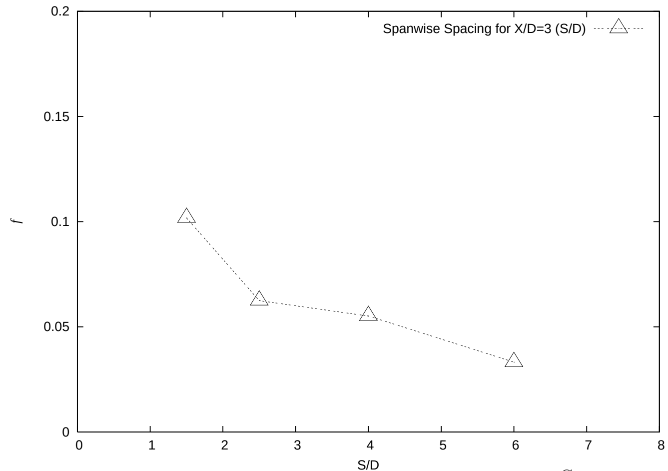

Figure 7–9: Dependence of the friction factor on $\frac{S}{D}$ and $Re = 4000$.

The Nu at the endwalls shows dependence on the spanwise space as well as on the Re. Figure 7–10 shows the dependence on both factors and a comparison with literature. As the spanwise space augments the Nu at the surface decreases due to the decrease of the perturbations of the flow in the section (fig. 7–10 a). It is well known that as the Re increases the Nu increases for a duct flow. Pin fins as promoters of disturbances in the flow augments the heat transfer in the surface as the Re increases (fig. 7–10 b). The Nu is lightly lower than the experiments, but as stated by [16] there is about 10% of variation in the data dispersion. The heat transfer augmentation in the endwall is also dependent on the Re and on the spanwise distance. The augmentation $\left(\frac{Nu}{Nu_0}\right)$ is shown in figure 7–11. In the case of the spanwise spacing variation the augmentation shows a decreasing trend as the space is increased (fig. 7–11 a). On the ohter hand the augmentation of the heat transfer decreased as the Re increased.

The friction factor, shown in figure 7–9, shows a decreasing trend as the spanwise spacing is increased. The decreasing in the friction factor is due to the reduced blockage effect that the downstream rows produce to the flow. As explained in the previous chapter the friction is due to the drag generated at the pin fins therefore the less pins per area the less the friction factor. From experiments it was concluded that as the Re was increased the friction factor decreases. The same result is obtained

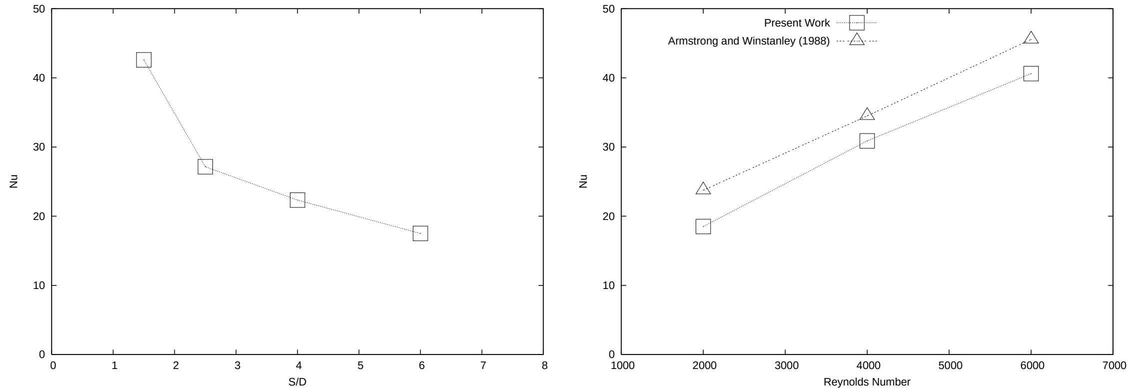

a) b)

Figure 7–10: (a) Dependence of the endwall Nusselt number on $\frac{S}{D} = 2.5$ for $Re = 4000$. (b)Dependence of the Nu on Re for $\frac{S}{D} = 2.5$ and $\frac{X}{D} = 1.5$ compared with [5] (experimental).

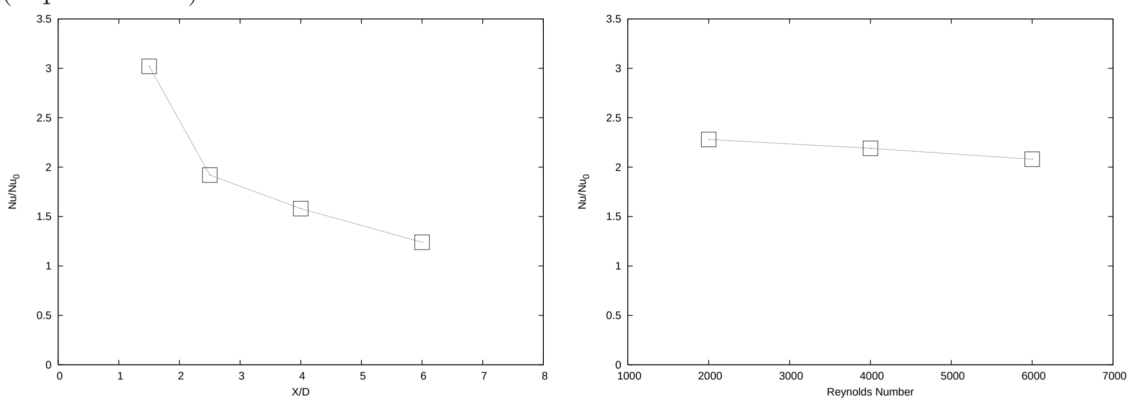

a) b)

Figure 7–11: (a) Dependence of the Nusselt number augmentation on $\frac{S}{D} = 2.5$ for $Re = 4000$. (b)Dependence of the Nu augmentation on Re for $\frac{S}{D} = 2.5$ and $\frac{X}{D} = 1.5$

from the simulations even though the Re range is lightly lower than the experiments (fig. 7–12) and Metzger et. al. [4].

To have a better appreciation of the combined effect of the heat transfer and the friction factor the ratio between both have been taken. Figure 7–13 a) shows that as the spanwise space becomes larger the ratio first start to decrease and then increases. This is because the cases studied with $\frac{S}{D} > 3$ have approximately the same heat transfer, but the friction factor is lower for the larger case ($\frac{S}{D} = 6$). This means that this configuration is more efficient not because it promotes a greater heat transfer but because it have a low friction factor than the other cases. For a fixed geometry the heat transfer to friction factor ratio (fig. 7–13 b)) decreases

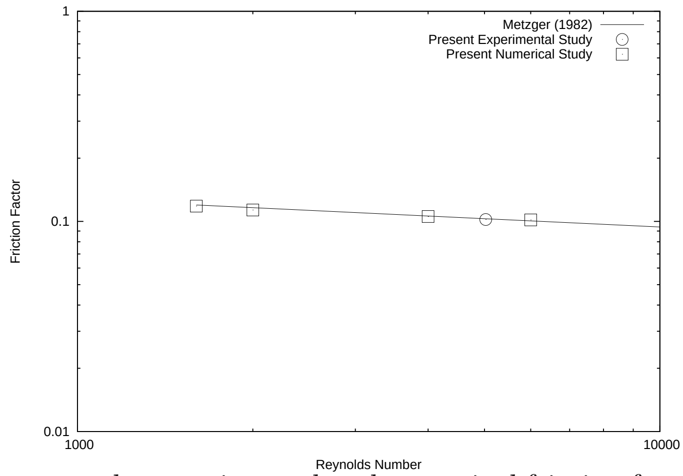

Figure 7–12: Present study experimental and numerical friction factor results plotted along with Metzger et. al. [4] correlations.

smoothly as the Re increases. From the results it is known that both factors, the heat transfer and the friction, decreases as the Re increases, but this ratio shows that the heat transfer rate decreases more rapidly than the friction factor.

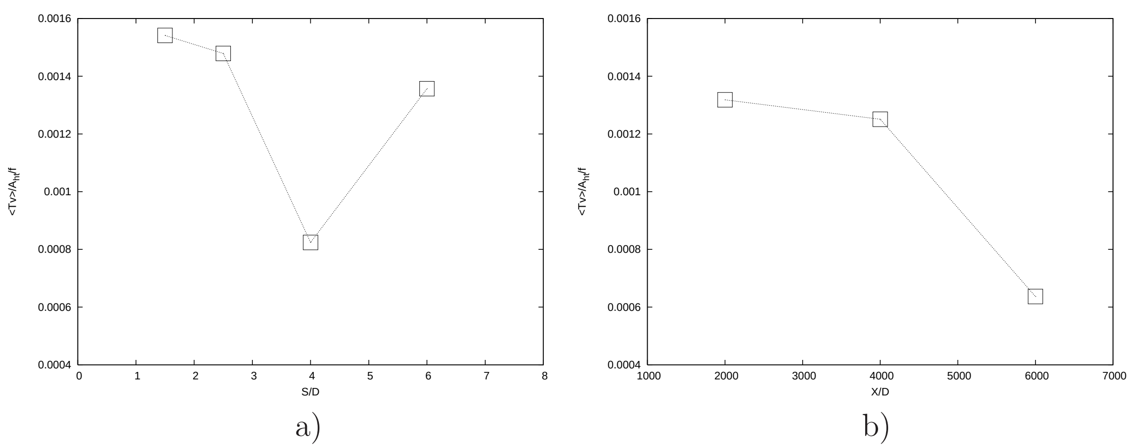

Figure 7–13: (a) Dependence of heat transfer to friction factor ratio on $\frac{S}{D}$ for Re. (b)Dependence of heat transfer to friction factor ratio on Re for $\frac{S}{D} = 2.5$ and $\frac{X}{D} = 1.5$.

The parametric study of the spanwise distance effect on the heat transfer and friction factor of a pin fin array shows that the most efficient configuration is $\frac{S}{D} = 2.5$ and $\frac{X}{D} = 3$, because it offers a heat transfer to friction factor ratio greater than the other two configurations. In case of the fixed configuration the Re with the maximum heat transfer to friction factor ratio is 2000.

7.2 Concluding Remarks

The time averaged velocity contours show that there is a net effect in the flow when the spanwise spacing and the Re are changed. The effect of increasing the spanwise spacing is that the localized high velocity between the pin fins is gradually loss. The blockage effect is lost as the spanwise space is augmented, when the space was very large the pin fins behaved more independently. For the closer spacing ($\frac{S}{D} = 1.5$) the wake from the upstream pin fins interact with the downstream row promoting turbulence which enhances the heat transfer. As the spanwise spacing between the pins increases the wake interaction is less ineffective.

For the same geometry the wake length is reduced as the Re increases. This is due to the larger high velocity zones at the side of the pin fins that enters the space between the rows. Instantaneous flow visualizations show localized high velocity zones at the region between the pins. For $Re = 4000$ the high velocity zones can not be appreciated since the shedding of all the pins is parallel and the flow is evenly distributed along the channel. This lead to the conclusion that the heat transfer changes as the flow sheds and this is a source of material creep.

Turbulent structures generated at the cylinder-endwall interface promote the convective heat transfer via the turbulent heat flux. The closer are the pin fins the higher the heat transfer per unit area. This is because the coherent structures interact with the downstream cylinders, but as the space is augmented the structures are dissipated and the heat transfer capabilities of the array are decreases.

The friction factor augments as the spanwise space is reduced. This is due to the blockage that the downstream rows imposes to the flow. As the spanwise space becomes larger the fluid is able to flow without many restrictions through the array reducing the resistance and therefore the friction factor. As the Re is increased for a fixed configuration the friction factor decreases, the same trend as [4]. With a higher Re the effect of the boundary layer in the friction factor is reduced and also the form drag is also reduced.

From this part of the present work it can be concluded that the configuration that promotes more heat transfer when varying the spanwise distance is $\frac{S}{D} = 1.5$, but this configuration also presents the highest friction factor. By augmenting the Re for a fixed configuration the heat transfer decreased, therefore the Re that promoted more heat transfer was 2000, but also presenting the highest friction factor. The efficiency of the array was measured by taking the ratio between the heat transfer and the friction factor. It was found that when varying the spanwise distance the most efficient configuration is $\frac{S}{D} = 1.5$ due to its higher heat transfer to friction factor ratio. In terms of the Re the most efficient is 2000, because the heat transfer decreases more rapidly than the friction factor.

CHAPTER 8
CONCLUSION AND RECOMMENDATIONS

The main objective of this work is to find the optimum layout for a pin fin array. The optimum configuration is the one that provides more heat transfer while giving the less friction factor. To understand how the flow affects the heat transfer and the friction factor and demonstrate the validity of the numerical code some experiments where performed before the pin fins numerical experiments. The experiments used to validate the numerical code where the infinite cylinder and the duct flow. The infinite cylinder results showed a very good resemblance with literature in terms of the drag coefficient (C_D), the wake length and the downstream flow behavior. For very low Re there was no separation of the flow from teh cylinder surface, as the Re was increased two attached eddies appeared at the trailing edge, and for higher Re the eddies disattach and the wake oscillates with a discrete frequency (St) that matches literature correlations [2] with a minimum difference. The drag coefficient was computed from the integral of the pressure coefficient (C_P) around the cylinder surface and it was compared to the curve fit proposed in [24], a very small difference was found.

The duct flow experiment showed boundary layer development in the near wall region due to the no-slip condition imposed on the walls. In this experiment the mean flow velocity was compared with the instantaneous velocity showing a time dependent term of the velocity. This time dependent term is the product of the turbulence in the channel. The time averaged shear stresses at the walls were computed and therefore the friction coefficient (C_F) for the duct was also found. When the

C_F was compared to literature [18] it was found a minimum difference. These two experiments demonstrate the validity of the numerical code when solving channel flow and cylinder flow and give the confidence that it will solve the pin fin problem.

Experiments conducted at the Pennsylvania State University as part of the present work showed that the friction factor normalized by the number of rows (f) tends to have a dependence on the Re and the number of rows. For one and two rows f increases as the Re increases. For three and four rows it increases, reaches a maximum, and start to decrease as the Re increases. Finally, for five to ten rows f decreases as the Re increases. Experimental results were also validated with past studies of Metzger et. al. [4]. It was also found that as the number of rows increased the pressure drop contribution due to the pin fins and the total pressure drop in the test section ratio converge to approximately 90% and the ratio losses the dependency on the Re. Experiments demonstrated that for more than six rows f followed the same trend and this was used as a stand point for the periodic boundary conditions of the numerical code.

The friction factor obtained from the simulations were compared with the past studies of Metzger et. al. [4] finding a very good fitting between the DNS data and the past study. Friction factor decreases as the streamwise space between the pin fins is increased, this is due to the blockage that the downstream rows create to the flow since they are staggered. The flow is able to reattach and dissipates the turbulence before reaching the next row this contributes to the friction factor reduction. Also by increasing the spanwise spacing and the Re the friction factor is reduced. In the case of the spanwise spacing the flow is able to flow more freely through the channel for larger spacings. As the Re increases the friction factor decreases since the form drag is the major contributor to the friction factor. It is known from the infinite cylinder that as the Re increases the drag decreases and pin fins are not the exception.

Friction factor is not the only characteristic that is affected by the spacing of the pin fins and the Re, the heat transfer is also affected. The results shows that the streamwise spacing imposes more effect on the heat transfer than the spanwise spacing. As the streamwise space is increased the heat transfer is reduced because there is less interaction between the coherent structures formed at the cylinder-endwall interface with the downstream rows. These coherent structures are responsible for enhancing the heat transfer in the near wall region and when the downstream distance is large they dissipate. On the other hand, as the spanwise spacing is increased the heat transfer decreases until it reaches a constant value. This is because the interaction between the adjacent pin fins is loss and the fluid flows freely through the array. For a fixed configuration the Re have an effect on the heat transfer. As the Re increases the heat transfer decreases due to the separation of the boundary layer and the flow configuration, this is in agreement with [12, 38]. Pin fins augment the heat transfer from 1.24 to 2.28 time more than the plain channel.

The efficiency of the pin fin array was computed as the ratio between the convective heat transfer and the friction factor. When the streamwise space was varied it was found that the most efficient configuration is $\frac{S}{D} = 2.5$ and $\frac{X}{D} = 3$. This configuration provides almost the same convective heat transfer as $\frac{X}{D} = 1.5$ but with a reduced friction factor. In case of spanwise variation the most efficient layout is $\frac{S}{D} = 1.5$ and $\frac{X}{D} = 3$. This configuration provide the maximum heat transfer to friction factor ratio when compared with greater spanwise spacings. The two test for spacing variation demonstrated that the most efficient configuration is $\frac{S}{D} = 1.5$ and $\frac{X}{D} = 3$ which provides the highest turbulent heat flux per unit area to friction factor ratio. When the Re was varied for $\frac{S}{D} = 2.5$ and $\frac{X}{D} = 1.5$ the Reynolds number with the highest efficiency is 2000. This Re provides the maximum heat transfer as well as the maximum friction factor but it demonstrate that the heat transfer decreases faster than the friction factor as the Re is increased.

8.1 Recommendations

The results from this work can be used depending on the type of goal the researcher is looking for, i.e. to increase the heat transfer or reducing the friction on the turbine blades. It also can serve as a base for improving turbulence models for future simulations using Reynolds Average Navier-Stokes (RANS). Since the data is explicit for each point the Reynolds stresses of the flow can be computed as well as correlated. The heat transfer analysis can be improved by adding the effects of conduction to the pin fins and also the buoyancy effects of temperature on the flow. The coherent structures formed at the cylinder-endwall interface can be studied in more detail to find their source and propagation downstream the channel. Finally, to have a more realistic feature rotation to the geometry can be added as a body force. For more realistic results endwall fillets can be added, and observe how the heat transfer and the friction factor varies when compared with the present work. Heat transfer can also be studied with the added effect of roughness on the channel area that is not covered by the pin fins.

REFERENCE LIST

[1] Orlandi P. *Fluid Flow Phenomena, a numerical toolkit*. Kluwer Academic Publishers, 2000.

[2] Tritton D. J. Experiments on flow past a circular cylinder at low reynolds number. 1959.

[3] Lyall M. E. and Thrift A. A. Heat transfer from low aspect ratio pin fins. *ASME Paper GT-2007-27431.*, 2007.

[4] Metzger D. E., Fan Z. X., and Shepard W. B. Pressure loss and heat transfer through multiple rows of short pin fins. *Heat Transfer*, 3:137–142, 1999.

[5] Armstrong J. and Winstanley D. A review of staggered array pin fin heat transfer for turbine cooling applications. *ASME Journal of Turbomachinery*, 110:94–103, January 1988.

[6] Metzger D. E., Fan C. S., and Haley S. W. Effects of pin shape and array orientation on heat transfer and pressure loss in pin fin arrays. *Journal of Engineering for Gas Turbines and Power*, 106:252–257, January 1984.

[7] Chyu M. K., Hsing Y. C., Shih T. I.-P., and Nataran V. Heat transfer contributions of pins and endwall in pin-fin arrays: Effects of thermal boundary condition modeling. *Journal of Turbomachinery*, 121:257–263, April 1999.

[8] Koşar A., Mishra C., and Y. Peles. Laminar flow across a bank of low aspect ratio micro pin fins. *Journal of Fluids Engineering*, 127:419–430, May 2005.

[9] Uzol O. and Camci C. Heat transfer, pressure loss and flow field measurements downstream of staggered two-row circular and elliptical pin fins arrays. *Journal of Heat Transfer*, 127:458–471, 2005.

[10] Ames F. E., Dvorak L. A., and Morrow M. J. Turbulent augmentation of internal convection over pins in staggered pin fin arrays. *ASME Turbo Expo GT-2004-53889*, 2004.

[11] Goldstein R. J., Jabbary M. Y., and Chen S. B. Convective mass transfer and pressure loss characteristics of staggered short pin-fin arrays. *International Journal of Heat and Mass Transfer*, 37:149–160, 1994.

[12] Peng Y. Heat transfer and friction loss characteristics of pin fin cooling configuration. *ASME Paper 83-GT-123*, 1983.

[13] Chen Z., Li Q., Meier D., and Warnecke H. J. Convective heat transfer and pressure loss in rectangular ducts with drop-shaped pin fins. *Heat and Mass Transfer*, 33:219–224, 1997.

[14] Şara O. N. Performance analysis of rectangular ducts with staggered square pin fins. *Energy Conversion & Management*, 44:1787–1803, 2003.

[15] Ames F. E. and Dvorak L. A. Turbulent transport in pin fin arrays - experimental data and predictions. *ASME Turbo Expo GT2005-68180*, 2005.

[16] Han J. C., Dutta S., and Ekkad S. V. *Gas Turbine Heat Transfer and Cooling Technology*. Taylor and Francis, 1999.

[17] Metzger D. E. and Haley S. W. Heat transfer experiments and flow visualization for arrays of short pin fins. *ASME Paper No. 82-GT-138.*, 1982.

[18] Munson B. R., Young D. F., and Okiishi T. H. *Fundamentals of Fluid Mechanics*. John Wiley and Sons, Inc., 2002.

[19] Incropera F. P. and DeWitt D. P. *Fundamentals of Heat and Mass Transfer*. John Wiley and Sons, Inc., 2002.

[20] Kim J. and Moin P. Application of a fractional-step method for incompressible navier-stokes equations. *Journal of Computational Physics*, 59:308–323, 1985.

[21] Kundu Pijush K. *Fluid Mechanics*. Academic Press, 1990.

[22] Dennis S. C. R. and Chang Gau-Zu. Numerical solutions for steady flow past a circular cylinder at reynolds number up to 100. *Journal of Fluid Mechanics*, 42:471–489, 1970.

[23] Roshko A. Experiments on flow past a circular cylinder at very high reynolds number. 1961.

[24] White Frank M. *Viscous Fluid Flow*. McGraw-Hill, Inc., 2nd edition, 1991.

[25] Bertin J. J. *Aerodynamics for Engineers*. Prentice Hall, 2002.

[26] Gunter A. Y. and Shaw W. A. A general correlation of friction factors for various types of surfaces in crossflow. *ASME Transactions*, November, 1945.

[27] Metzger D. E., Berry R. A., and Bronson J. P. Developing heat transfer in rectangular ducts with staggered arrays of short pin fins. *Journal of Heat Transfer*, 104:700–706, November 1982.

[28] Chyu M. K. Heat transfer and pressure drop for short pin-fin arrays with pin-endwall fillet. *Journal of Heat Transfer*, 112:926–932, November 1990.

[29] Chang B. H. and Mills A. F. Effect of aspect ratio on forced convection heat transfer from cylinders. *International Journal of Heat and Mass Transfer*, 47:1289–1296, 2004.

[30] Frederich O., Wassen E., and Thiele F. Prediction of the flow around a short wall-mounted finite cylinder using les and des. *Journal of Numerical Analysis, Industral, and Applied Mathematics*, 3:231–247, 2008.

[31] Goldstein R. J., Chyu M. K., and Hain R. C. Measurements of local mass transfer on a surface in the region of the base of a protruding cylinder with a computer-controlled data acquisition system. *International Journal of Heat and Mass Transfer*, 28:977–985, 1985.

[32] Sparrow E. M. and Ramsey J. W. Heat transfer and pressure drop for a staggered wall-attached array of cylinders with tip clearance. *International Journal of Heat and Mass Transfer*, 21:1369–1377, 1978.

[33] Furuya Y., Miyata M., and Fujita H. Turbulent boundary layer and flow resistance on plates roughened by wires. *Journal of Fluid Engineering*, 98:635–644.

[34] Arora S. C. and Abdel-Messeh W. Characteristics of partial length circular pin fins as heat transfer augmentors for airfoil internal cooling passages. *ASME Paper 89-GT-87.*, 1989.

[35] Damerow W. P., Murtaugh J. C., and F. Burgraf. Experimental and analytical investigation of the coolant flow characteristics in cooled turbine airfoils. *NASA CR-120883*, 1972.

[36] Cruz Perez B., Toro Medina J., Sundaram N., Thole K., and Leonardi S. Direct numerical simulation and experimental results of a turbulent channel flow with pin fins array. *Direct Large Eddy Simulations 7*, 2008.

[37] Jeong J. and Hussain F. On the identification of a vortex. *Journal of Fluid Mechanics*, 285:69–94, 1995.

[38] G. Theoclitus. Heat-transfer and flow-friction characteristics of nine pin-fin surfaces. *Journal of Heat Transfer*, pages 383–390, November 1966.